ELSEVIER

International Journal of Mass Spectrometry 200 (2000) 97–136

International Journal of Mass Spectrometry

Experimental studies of positive ion chemistry with flow-tube mass spectrometry: birth, evolution, and achievements in the 20th century

Diethard K. Böhme*

Department of Chemistry, Centre for Research in Mass Spectrometry, Centre for Research in Earth and Space Science, York University, Toronto, Ontario M3J 1P3, Canada

Received 6 July 2000; accepted 14 August 2000

Abstract

Flow-tube mass spectrometry as a technique to measure positive ion–molecule reactions is tracked from its birth to the beginning of the 21st century. Major achievements in the development and the application of this technique are surveyed. The instrumental developments that are considered include advances in ion production and selection, neutral introduction, temperature and energy control in the flow reactor and the detection and probing of product ions and neutrals. Emphasis is given to the use of flow-tube mass spectrometry in measurements of the dependence of ion reactivity on temperature, kinetic energy and internal energy. Achievements in our understanding of basic reaction types are discussed, including electron-transfer, proton-transfer, metal, and organometallic ion reactions and electron–ion recombination. A review is included of fullerene–ion chemistry that has been a focus in the laboratory of the author at York University over the last 10 years. Finally, the progress made in ionospheric and interstellar/circumstellar chemistry, historically the two main areas of application, and the more recent application of flow-tube mass spectrometry in analytical/medical chemistry are highlighted. (Int J Mass Spectrom 200 (2000) 97–136) © 2000 Elsevier Science B.V.

Keywords: Flow-tube mass spectrometry; Positive-ion chemistry

1. Foreword

Of course I was delighted to be asked to contribute to this benchmark volume on the state of mass spectrometry and ion chemistry at the turn of the 20th century. The use of flow-tube mass spectrometry to study ion chemistry has provided me with many thrills and much satisfaction in my research activities over the years and I welcome this unique opportunity to provide a personal perspective. I was given the directive to review the field of flow-tube mass spectrometry from its beginning to the end of the 20th century, not exhaustively but rather by capturing the essence of the major developments in this field and the breadth of its achievements. I was asked to restrict myself to positive-ion chemistry and developments of the technique itself and I was encouraged to give emphasis to my own research. Chuck DePuy has been asked to survey negative-ion chemistry. So our two contributions should be viewed in combination to

* E-mail: dkbohme@yorku.ca

Dedicated to Eldon Ferguson, a pioneer par excellence.

PII S1387-3806(00)00299-2

appreciate the full impact of flow-tube mass spectrometry on ion chemistry.

2. Birth

Flow-tube mass spectrometry was born in the early 1960s. As it happened, I was totally engrossed at the time in my Ph.D. research with Professor John Goodings at McGill University in Montreal where we were constructing a quadrupole mass spectrometer, the first of its kind in Canada, to be used to sample ions from a Lewis-Rayleigh nitrogen afterglow plasma [1]. We had just visited John Paulson at the Air Force Cambridge Research Laboratories near Boston in the United States. John kindly provided us with a gold-plated (!) quadrupole mass filter for use in my research (my contribution was to design and construct the necessary power supply). Rocket-borne quadrupole mass spectrometers already were being used by Rocco Narcissi and his colleagues at Air Force Cambridge to explore naturally occurring ions in the earth's ionosphere in response to a mission in radio propagation initiated by the US National Bureau of Standards (NBS) [2]. At about the same time, elsewhere in the US, Eldon Ferguson, together with Art Schmeltekopf and Fred Fehsenfeld (two of Eldon's graduate students at the University of Texas, Austin) had been hired by NBS to create a laboratory aeronomy program at the Environmental Science Services Administration (now the National Oceanic and Atmospheric Administration) in Boulder, CO. Art Schmeltekopf had just spent time with Herb Broida in Washington performing optical spectroscopic measurements on a "flowing afterglow" initiated by a microwave discharge in a large glass tube exhausted with a very large Roots Blower pump. A similar system was set up in Boulder, but it was connected to a homebuilt quadrupole mass spectrometer. So one day, in the quiet (dry) town of Boulder, CO, air leaked into discharged helium carrier gas and N^+ revealed itself to the quadrupole mass spectrometer. Eldon, Art, and Fred quickly realized that this ion could only have come from the dissociative ionization reaction of N_2 with He^+. A simple analysis of the gas-flow dynamics then led these three, together with Harold Schiff who was visiting at the time, to the realization of the possibility to do quantitative chemical kinetics. So a powerful and versatile technique for the observation and measurement of ion–molecule reactions was born. Eldon has recounted these early special moments in his personal recollections of the birth of what became known as the flowing-afterglow (FA) technique [3]. The subsequent use of the FA technique for measurements of ion–molecule reactions was thoroughly documented by Eldon, Fred, and Art in 1969 [4]. This benchmark article includes a detailed description of the basic apparatus (see Fig. 1), an analysis of the gas flow including radial and axial diffusions, a discussion of inlet effects and an analysis of ion–molecule reaction kinetics.

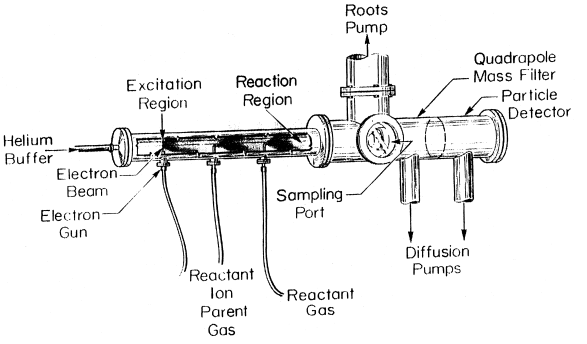

Fig. 1. Pictorial presentation of the early flowing-afterglow mass spectrometer [4].

The basic FA technique is conceptionally simple: ions are introduced into a flowing bath gas at room temperature and a pressure in the range from 0.2 to 1.0 Torr, allowed to thermalize by collisions with bath gas atoms or molecules (or reacted first with an added gas to chemically alter their identity), allowed to react with added neutral atoms or molecules, and then sampled and monitored along with product ions as a function of the added reactant. Time usually is replaced by reactant concentration as the kinetic variable by adding the reactant in variable amounts at a fixed position in the flow tube. However, the key feature associated with the FA technique is the spatial separation of the ion production, ion thermalization, ion reaction, and ion detection regions. It is this

"modular" feature that is responsible for the exceptional versatility of the technique and accounts for its enormous success. To be sure, the early design of the FA mass spectrometer has evolved with time to further enhance the range of possible measurements and to considerably expand the applications of flow-tube mass spectrometry, but always without sacrificing spatial separation.

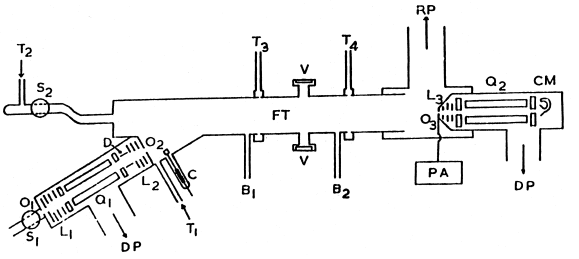

Fig. 2. Schematic diagram of the selected-ion flow-tube (SIFT) apparatus [6].

3. Evolution

Numerous applications were inspired by the basic FA technique, reaching far beyond the study of ionospheric chemistry for which it was originally conceived. Many technical advances in flow-tube mass spectrometry accompanied these applications. Those reported up to 1988 have been thoroughly documented in the superb review article of Graul and Squires [5]. This review is a most valuable resource and includes a detailed discussion of the design and evolution of ion sources, flow tubes and methods of ion detection that have been employed in the application of flow-tube mass spectrometry. Here I will only briefly outline some of the key features of the technique and report briefly on the technical advances made since 1988.

3.1. Ion production and selection

In the earliest version of the flow tube, ions were generated directly from a chosen parent gas upstream within the flowing bath gas in an afterglow plasma energized with an electron filament that generated electrons, metastable atoms, as well as positive and negative ions [4]. Extra versatility is provided by the ability to further manipulate the identity of the ions produced in this way simply by allowing the ions to react chemically with another added gas prior to entering the reaction region. With the development of the selected-ion flow tube (SIFT), ions of interest could be created in an ion source external to the flow tube, mass selected, and injected into the carrier gas by means of a Venturi inlet [6,7]. This development was a major breakthrough since ions now could be introduced into the flow tube in the absence of other interfering charged, metastable and neutral molecules (see Fig. 2). Now the extraordinary utility of the flow-tube technique for the measurement of the reactivity of ions became limited only by the versatility of the ion source used to generate specific ions upstream of the selection quadrupole and Venturi inlet.

A large variety of ionization sources have been coupled to the flow tube in either the FA or SIFT configurations and these have for the most part been thoroughly discussed by Graul and Squires [5]. They include low-pressure electron-impact ionization and high-pressure chemical-ionization sources that employ electron-emission filaments, microwave and dc discharges, the use of a flowing afterglow itself as an ion source, and the production of various atomic metal-ions by electron impact on metallic vapours, with thermionic emission filaments or by eximer laser vaporization of metal targets. Dedicated sources have also been developed for cluster ions. A high-pressure FA source separated from the flow-tube region by a diaphragm containing a small orifice was used by Viggiano and co-workers in 1988 to study reactions of hydronium ions hydrated with up to eleven water molecules [8]. The source design was based on the one originally used by Fahey and co-workers in the study of chemistry of hydrated negative ions [9]. In 1991 Castleman and co-workers employed such a source to produce hydrated-hydronium ions, $H_3O^+(H_2O)_n$ with n as large as 60 [10]! Much more recently Viggiano and co-workers have incorporated a supersonic expansion ion source for cluster-ion production at low temperatures. Greater versatility is

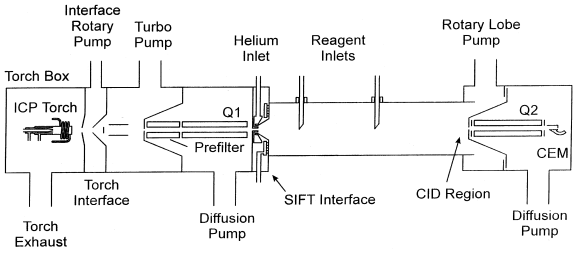

Fig. 3. Schematic diagram of the ICP/SIFT apparatus [15].

achieved by entraining an additional gas in the expansion and by allowing conversion to the cluster ion of choice [11].

More recently Squires has combined the flow-tube technique with in situ electrospray ionization [12]. Ions can be electrosprayed from a high-voltage syringe needle directly into the flow tube through a foot-long heated capillary without the need for differential pumping or ion focusing and without the reclustering of the desolvated ions with the background solvent vapour. The electrospray source has been used to good effect very recently in the study of ion–molecule reactions of protonated glycine [13] including H/D exchange reactions [14].

At York University we have recently interfaced our SIFT with an inductively coupled plasma (ICP) originally developed for elemental and isotopic analysis [15]. The plasma operates at a temperature of ~6000 K and provides in essence a universal source for atomic ions, although selected atomic oxide ions and doubly charged atomic ions also can be produced. The ICP requires only the injection of a dilute solution of a compound containing the atom of interest, can be run continuously, even for months at a time, and allows rapid switching from one atomic ion to another simply by changing the solution! However, as the conventional ICP operates at atmospheric pressure, a differentially pumped interface is required to allow plasma-ion sampling. The ICP/SIFT configuration (see Fig. 3) allows the routine measurement of fundamental aspects of reactions of atomic and atomic oxide ions with neutral molecules of essentially any atom on the periodic table.

3.2. Neutral introduction

The neutral reagents enter the flow tube from an external source and so the nature of a neutral reagent is limited only by the versatility of its mode of production. This was demonstrated early in a stunning experiment involving the reaction of vibrationally excited N_2 with O^+ as a function of the vibrational excitation [16]. Stable gases, vapours of liquids and solids, and a large variety of unstable species have been employed as reagents over the years of use of flow-tube mass spectrometric techniques. Graul and Squires have reviewed in detail the various methods employed for controlling reagent flows, enhancing transfer of low-volatility compounds, and producing unstable species including atomic and molecular radicals, vibrationally hot reagents, and metastable electronically excited species [5]. There has not been significant further innovation since 1988 in this regard. Graul and Squires also have drawn attention to advantages inherent in the flow technique with regard to maintaining the integrity of added neutrals, particularly unstable neutrals. Ion atom chemistry, the first example of which was reported by Ferguson et al. in 1965 [17], is currently being actively pursued in the laboratory of Murray McEwan at the University of Christchurch [18].

3.3. Ion flow reactor/temperature control/energy control

Whether reactant ions are produced within the flow tube or introduced from an external source, they are subsequently thermalized by collisions with bath gas atoms when they enter the flow tube. This ensures the energy definition of the reacting ions prior to reaction and that the subsequent reaction proceeds at the temperature of the bath gas. The bath gas temperature is determined by the tube temperature, which is normally in thermal equilibrium with room temperature.

Although most rate measurements with flow reactors have been made only at room temperature, temperature dependencies often have been of interest and instrumental modifications have been developed

to allow measurements as a function of temperature. This was already achieved during the 1960s in Boulder, CO. Ferguson and his colleagues wanted to simulate the temperatures found naturally in the earth's ionosphere and so constructed a flow-tube mass spectrometer designed to operate over the temperature range from 80 to 600 K [19] which was then extended up to 900 K [20]. In order to further understand high temperature plasmas and combustion, Viggiano and colleagues constructed a high temperature flowing afterglow (HTFA) for studying ion–molecule reactions at temperatures from 300 to 1800 K [21,22]. Variation in temperature has been combined with SIFT operation in the construction of a variable-temperature selected-ion flow-tube (VT-SIFT) apparatus designed to operate between 80 and 550 K [23].

A flow-drift tube technique was introduced by Ferguson and his colleagues in 1973 to allow ion mobility and ion–molecule reaction measurements as a function of reactant ion/reactant neutral center-of-mass kinetic energy [24]. Molecular ions drifting at elevated E/N (where E is the electric field strength and N the buffer gas density) were shown to become vibrationally excited. It became possible to study (1) the excitation and de-excitation of molecular ions in collision with the buffer gas (including Ar, Ne, and N_2), (2) the quenching of vibrationally excited ions in collision with various neutrals, and (3) the role of ionic vibrational excitation in ion–molecule reactions [25]. It did not take long for the flow-drift operation to be combined with SIFT operation in the construction of a SIFT-drift tube (SIFT-DT) apparatus and so to do these measurements with selected ions [26].

The ultimate combination of the capabilities of the variable-temperature flowing afterglow, the flow drift tube and the SIFT was reported in 1979 by Smith and Adams [27] and is shown in Fig. 4. The first results with this technique on the isotopically labeled switching reaction of N_4^+ with N_2 was published 1n 1984 [28].

3.4. Product ion/neutral detection/probing

A quadrupole mass filter/electron multiplier configuration was employed in the original FA apparatus

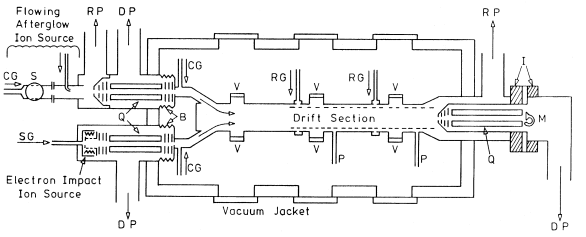

Fig. 4. Schematic diagram of the variable-temperature, SIFT, flow drift-tube mass spectrometer, or VT-SIFDT [27].

to mass select reactant and product ions and to determine their relative concentrations. The ions were sampled at a nose-cone voltage near 0 V. Direct in situ measurements of ion and electron densities became possible with the application of the Langmuir probe technique by the group in Birmingham [29,30]. This flowing afterglow/Langmuir probe (FALP) technique became invaluable for the measurement of ion–electron and ion–ion recombination coefficients. Direct information about excited ions became accessible with a magnetic resonance technique developed to measure the polarization of emissions from excited ions produced from optically pumped metastable helium atoms [31].

Information on the structures and energetics of the ions themselves did not become available until Squires and his colleagues attached a triple quadrupole instrument to a FA apparatus [32]. This combination allowed the characterization of ion structures by tandem mass spectrometry (MS/MS) and ion energetics by energy-resolved collision-induced dissociation (CID). A few years later this instrument was upgraded to a SIFT-triple quadrupole instrument [33]

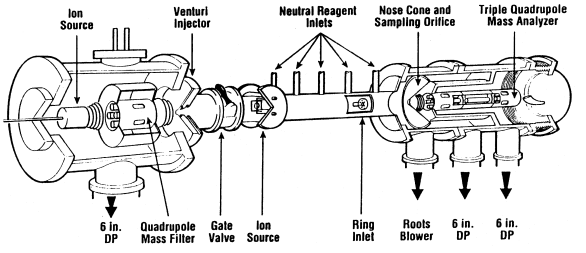

Fig. 5. Schematic view of the SIFT triple quadrupole mass spectrometer [32].

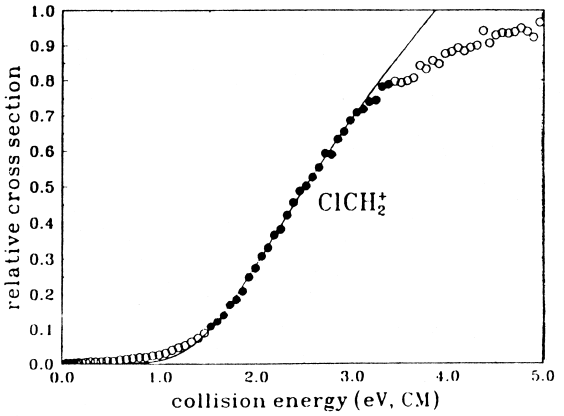

Fig. 6. Relative cross sections for CID of as a function of translational energy in the center-of-mass frame measured with the SIFT triple quadrupole mass spectrometer. The solid line is a theoretical fit over the range of the solid circled data points [33].

shown schematically in Fig. 5. Fig. 6 shows a CID threshold measurement that provided a value for the chloromethyl cation affinity of methyl chloride [33]

At York University we have recently developed an inexpensive, somewhat crude, but nevertheless effective, multicollision CID technique that has proven to be remarkably useful for the determination of bond connectivities and approximate bond energies and which often allows the discrimination between isomeric ions as illustrated in Fig. 7. Multicollision-induced dissociation is achieved by raising the potential of the sampling nose cone while retaining constant mass discrimination [34].

Detection of neutral and ionic products by optical spectroscopy and laser-induced fluorescence usually limited to diatomic and triatomic molecules has been reviewed by Graul and Squires [5], as has cryogenic trapping of neutral products that have been employed in a few selected instances.

4. Achievements

After the early flow-tube studies at ESSA in Boulder, CO directed to ionospheric chemistry, the scope of flow-tube measurements grew quickly also to embrace fundamentals of gas-phase ion kinetics and thermochemistry, physical-organic chemistry, atmospheric chemistry, interstellar/circumstellar chemistry, plasma chemistry, fullerene chemistry, analytical chemistry and ultimately even medical chemistry.

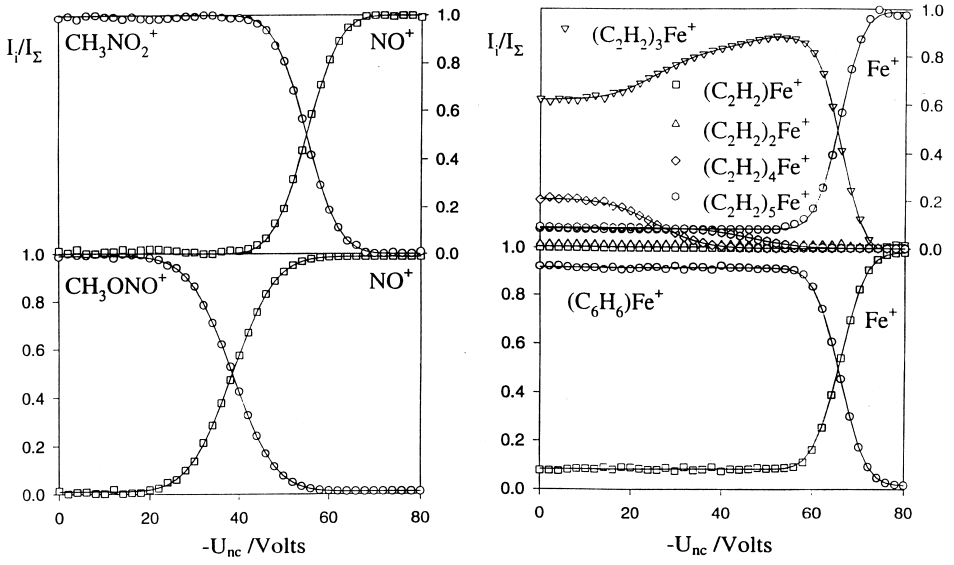

Fig. 7. (Left) Multicollision CID results for the isomeric ions $CH_3NO_2^+$ and CH_3ONO^+. (Right) Multicollision CID results for $(C_2H_2)_nFe^+$ and (benzene)Fe^+ ions providing the identification of $(C_2H_2)_3Fe^+$ as (benzene)Fe^+ [34].

This burst in applications is already very evident in the 1987 Festschrift issue [35] of the International Journal of Mass Spectrometry and Ion Processes dedicated to Eldon Ferguson, and also in the 1988 review of Graul and Squires [5].

I have chosen to organize the achievements in the following manner. Fundamental aspects of the kinetics of ion–molecule reactions are considered first, including flow-tube mass spectrometer measurements of the dependence of ion reactivity on temperature, kinetic energy and internal energy. Then studies of a number of basic reaction types are discussed, including electron-transfer, proton-transfer, metal, and organometallic ion reactions and electron–ion recombination. A separate section is included on fullerene–ion chemistry that has been a focus in our laboratory at York University over the last 10 years. Finally I have reviewed the progress made in ionospheric and interstellar/circumstellar chemistry, historically the two main areas of application, and the more recent application of flow-tube mass spectrometry in analytical chemistry.

Basic measurements: the basic data acquired in a flow-tube experiment involves the measurement of reactant and product ion profiles as a function of reactant flow at a fixed reaction time (or time at a fixed reactant flow). The application of conventional pseudo-first-order kinetics to the semilogarithmic decay of the primary reactant ion (in the absence of significant reverse reaction) allows the determination of the rate coefficient k_f of the primary reaction, but account must be taken of losses due to radial and axial diffusion and ambipolar diffusion if present. Fitting of higher-order ion profiles with solutions of appropriate kinetic equations can provide values for higher-order rate coefficients. Detailed kinetic analyses have been published including the determination of branching fractions for reactions with more than one product [4,36].

A primary reaction (1) may be induced to reverse with the deliberate addition of neutral backreactant D (see Fig. 8) [37].

$$A^+ + B \rightleftarrows C^+ + D \quad (1)$$

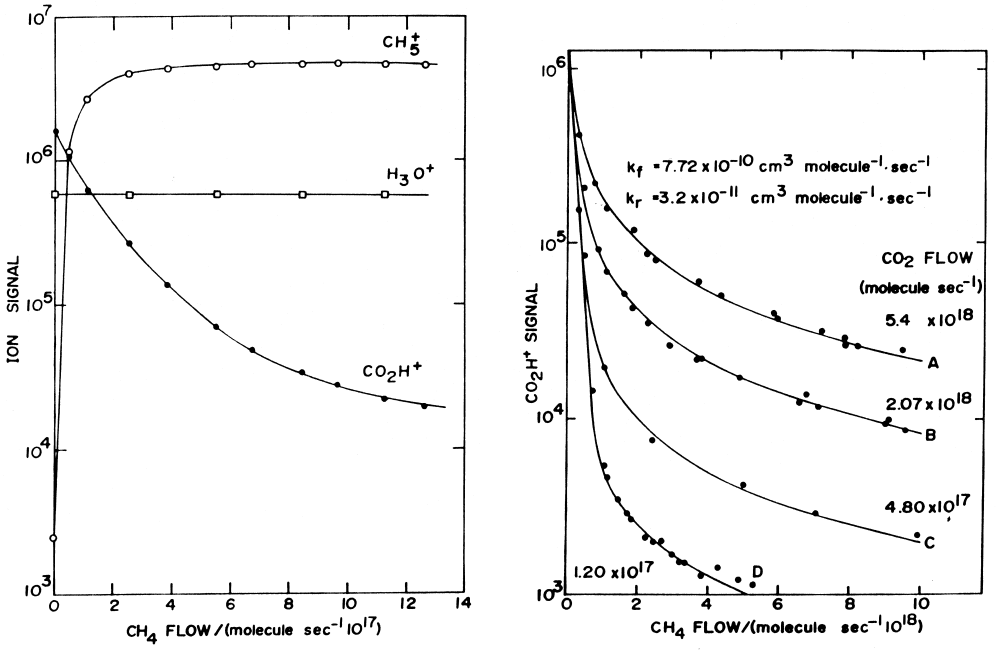

Fig. 8. (Left) Major ions present at various additions of methane into a flowing plasma in which CO_2H^+ is established as the dominant ion. The flow of CO_2 is 5.1×10^{17} molecules s^{-1} [37]. (Right) Variations in CO_2H^+ upon addition of methane at various flows of CO_2. Solid lines are fits with the values for the forward and reverse rate coefficients indicated [37].

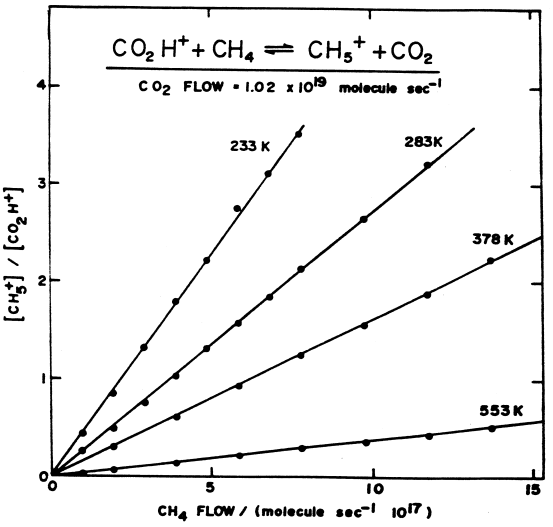

Fig. 9. Measured variation in the ratio of the reactant to the product-ion signal with the flow of neutral reagent at four different temperatures. The straight lines yield equilibrium constants of 46.8, 27.9, 16.4, and 6.8 at 233, 283, 378, and 553 K, respectively [38].

This can lead to achievement of equilibrium and the determination of the reverse rate coefficient k_r from a fit of what becomes a curved semilogarithmic decay, and thus the thermodynamic equilibrium constant $K = k_f/k_r$. Alternatively, the reverse reaction can be investigated independently. Also the approach to, and achievement of, equilibrium can be monitored in a plot of $[C^+]/[A^+]$ versus [B] when D is added in large excess and K can be determined from the achievement of linearity (see Fig. 9) [38]. Thus, in principle, measurements are possible for k_f and k_r or $(k_f/k_r)_{ne}$ under nonequilibrium conditions as well as $(k_f/k_r)_e$ and K under equilibrium conditions. If Maxwell-Boltzmann distributions hold for reactants and products $(k_f/k_r)_{ne}$, $(k_f/k_r)_e$ and K should be equal and this is usually assured under typical flow-tube conditions as a consequence of collisions with excess buffer-gas atoms.

5. Effects of temperature on chemical reactivity

Variations in rate coefficients, product distributions, and equilibrium constants all can be explored as a function of temperature using flow-tube mass spectrometer techniques. Past measurements have been directed toward their application in models of ionospheric, interstellar, combustion, and plasma chemistry generally, but also toward fundamental kinetic and mechanistic aspects of ion–molecule reactions. Many of the current measurements of temperature dependence are being conducted in the laboratory of Viggiano and his colleagues and these are driven greatly by interests in combustion and plasma chemistry.

The prevailing features of the temperature dependence of rate coefficients for positive ion–molecule reactions were identified early and are illustrated in Fig. 10 [39]. Reactions that are fast at room temperature are essentially temperature independent; they can be expected to follow the temperature dependence of the collision rate coefficient. For slower reactions the rate coefficient often decreases with temperature and this has been attributed to a decrease in the lifetime of the reaction complex with increasing temperature. At sufficiently high temperatures however, the rate coefficient often increases with temperature and this is to be interpreted in terms of the details of the potential-energy surfaces that describe the reaction. The ultimate experimental achievement so far is the measurement of the rate coefficient for

$$O^+ + N_2 \rightarrow NO^+ + N \qquad (2)$$

from 80 up to 1800 K [40]! For this reaction the rise at higher temperatures has been interpreted in terms of the influence of translational energy and the vibrational energy of nitrogen.

Important combustion reactions for which rate coefficients and branching ratios have been measured recently using a VT-SIFT apparatus up to 500 K include the reactions of air plasma ions with numerous alkanes [41,42] and aromatics [43–45]. The measurements have been extended to temperatures greater than 1000 K for reactions with benzene [43] and naphthalene [45] using the HTFA mass spectrometer. Measurements of equilibrium constants as a function of temperature have not been as extensive and have been performed largely for the determination of the relative proton affinities of molecules [37]. Fig. 11 shows the van't Hoff plot of equilibrium

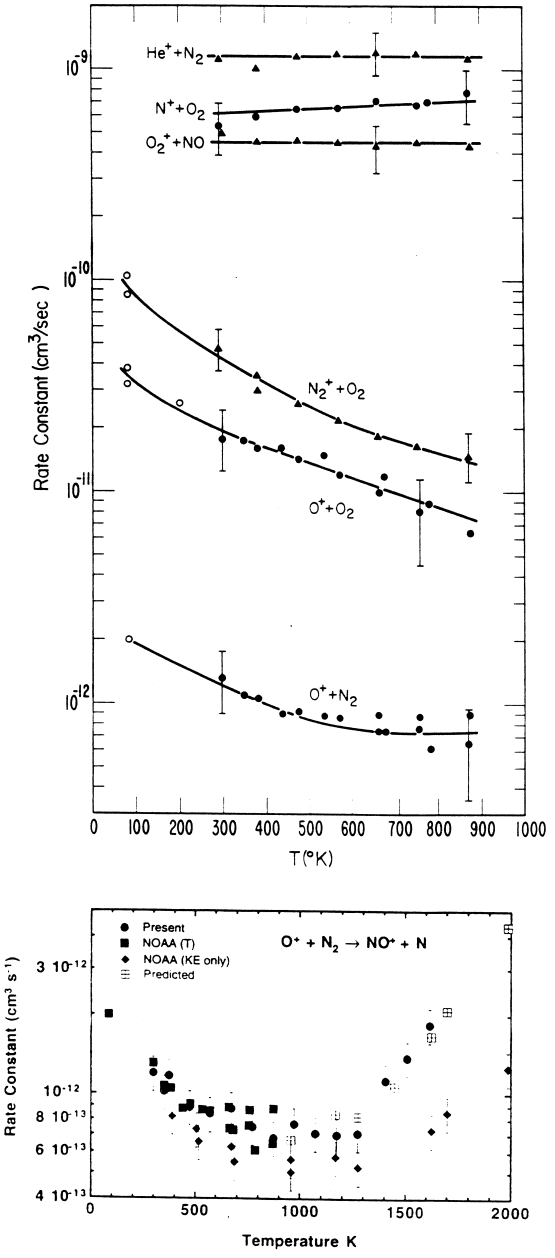

Fig. 10. (Top) Rate coefficients for several ionospheric reactions measured from 80 to 900 K [39]. (Bottom) Rate coefficients for the reaction of O^+ with N_2 measured from 80 to 1800 K [40].

constants measured for the transfer of a proton from CO_2H^+ to CH_4. Such plots of course are most useful for the determination of the thermodynamics of ion–molecule reactions.

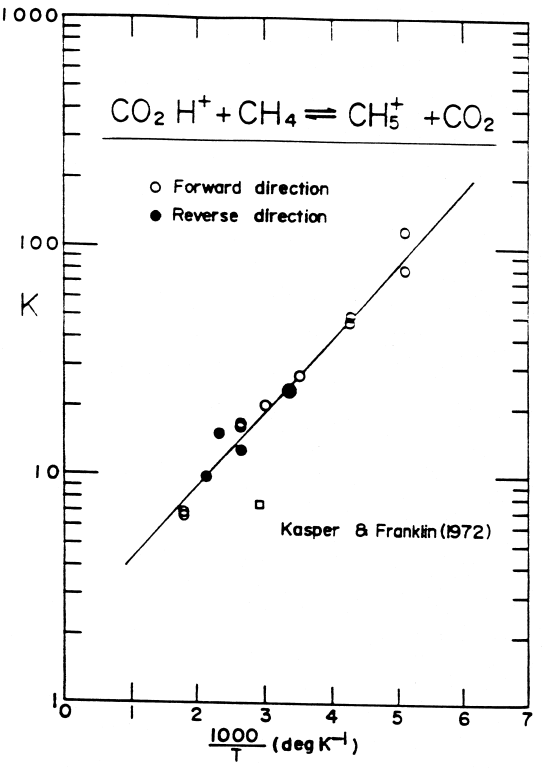

Fig. 11. A van't Hoff plot of equilibrium constants measured in the temperature range 196–552 K. A least-square fit to the data yields $\Delta H° = -0.064 \pm 0.004$ eV from the slope and $\Delta S° = +1.4 \pm 0.3$ e.u. from the intercept [37].

6. Effects of kinetic energy and internal energy (vibrations and rotations) on chemical reactivity

A variety of flow techniques have proven to be highly suited to the separate measurement of the effects of translational, rotational, and vibrational energy on chemical reactivity as documented in a recent review by Viggiano and Morris [46]. The original FA mass spectrometer was used early in a classic experiment that dramatically illustrated this point by measuring the influence of the vibrational energy of nitrogen (excited externally in a microwave discharge) in reaction (2) [16]. The extraordinary results of these measurements are shown in Fig. 12. With the development of the flow-drift tube came experiments that demonstrate the use of this technique with different buffer gases for measurements of the

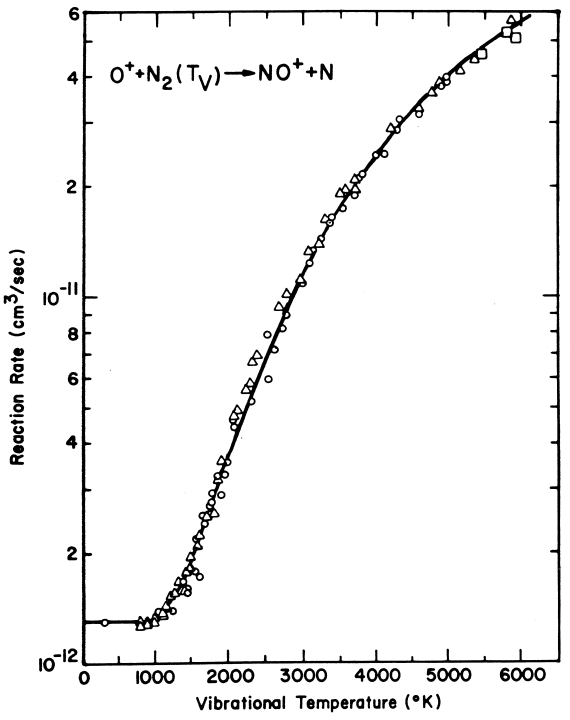

Fig. 12. Measurements of the variation of the rate coefficient for the reaction of $O^+ + N_2 \rightarrow NO^+ + N$ with the vibrational temperature of N_2 [16].

influence of vibrational energy on selected endothermic and exothermic proton-transfer and electron-transfer reactions [47]. A monitor-ion technique involving the judicious choice of monitor gas sensitive to the vibrational state of the ion was then developed that provides insight into the internal state of the ion chemically [48]. More detailed studies performed by Leone, Bierbaum, and colleagues have involved exciting the ion by varying the injection energy in a SIFT and monitoring the excitation by laser techniques [49].

The Variable Temperature-Selected Ion Flow Drift Tube (VT-SIFDT) technique allows the separate study of the effects of translational, rotational, and vibrational energy on chemical reactivity. The first such combined VT-SIFDT apparatus was used in early studies by Adams et al. [50] to investigate kinetic energy effects for the reactions of O_2^+ with CH_4 and CD_4,

$$O_2^+ + CH_4 \rightarrow CH_3O_2^+ + H \quad (3)$$

and to compare these to temperature effects leading to an empirical relationship, KE = *nkT*, to relate these two effects (see Fig. 13) [46]. This certainly is the ion–molecule reaction most thoroughly investigated with flow-tube mass spectrometry. In the most definitive study of this reaction to date, a mechanism and model has been developed to provide a fit to the observed temperature dependence and the agreement between theory and experiment is excellent [51].

More detailed and extensive studies were performed with the VT-SIFDT apparatus that was constructed in the Geophysics Laboratory, Hanscomb AFB [52]. Measurements with this apparatus focused on the influence of rotational and vibrational temperature on reactivity. In some instances the influence of individual vibrational energy levels was also unraveled [46]. Numerous reactions now have been investigated with this apparatus and a number of significant findings can be summarized in the words of Viggiano and Morris [46]: “Rotational and translational energy was found to be equally efficient in driving endothermic reactions. For exothermic reactions, large rotational effects are found only when one or both of the reagents have a large rotational constant. This indicates that changing from a low to moderate *J* value can affect reactivity but that changing from moderate to high *J* has little influence on reactivity. Vibrational effects are more varied. In some reactions vibrational excitation in the anticipated reaction coordinate strongly affects reactivity, while in other cases it does not.”

7. Electron transfer

The investigation of electron-transfer reactions (often termed charge transfer, although an electron actually is transferred) with flow-tube mass spectrometers also dates back to the early measurements directed toward ionospheric chemistry in which such reactions also participate. Particularly unique is

$$O^+ + H \rightarrow H^+ + O \quad (4)$$

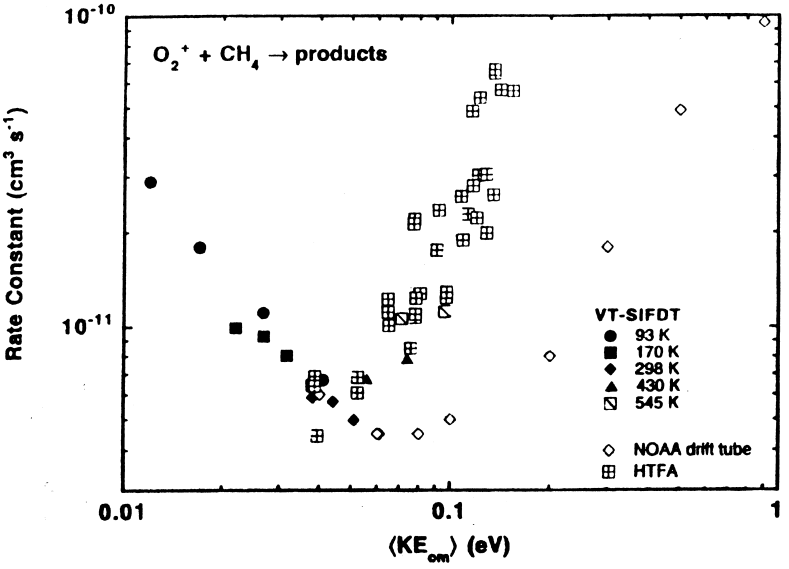

Fig. 13. Rate coefficients for the reaction of O_2^+ with methane measured as a function of average energy with a VT-SIFDT mass spectrometer. Also shown are data taken with DT and HTFA mass spectrometers [46].

the major source of H^+ in the ionosphere, in which electron transfer occurs by accidental near resonance because of the near equality of IE(O) and IE(H). The rate coefficients in the two directions of electron transfer have been found to be equal within a factor of 2 at 300 K, $k_4 = 6.8 \times 10^{-10}$ and $k_{-4} = 3.8 \times 10^{-10}$ cm^3 $molecule^{-1}$ s^{-1} [53]. The main loss of He^+ in the ionosphere is

$$He^+ + N_2 \rightarrow N^+ + N + He \quad (5a)$$

$$\rightarrow N_2^+ + He \quad (5b)$$

an example of (partial) dissociative electron transfer. The coefficient k_5 is large and independent of temperature between 300 and 900 K (see Fig. 10). The branching ratio, k_{5a}/k_{5b} (=0.7/0.3 at 300 K), increases with the nitrogen vibrational temperature but k_5 does not [54].

More recently, dissociative electron transfer per se, and the transition from nondissociative electron transfer to dissociative electron transfer, have become of interest for larger, organic molecules. The extent of dissociation can be managed by controlling the recombination energy of the reacting ion.

In a FA mass spectrometer study of Tsuji et al. electron-transfer products and rate coefficients were determined for reactions between thermal Ar^+ ions and lower alkanes and alkenes (C_1 to C_3) and C_2H_2 [55]. A comparison of the measured product distributions with photoelectron–photoion coincidence (PEPICO) spectra indicated that 85%–95% of the recombination energy was deposited in the molecular ion product. A SIFDT study in Lindinger's laboratory extended these measurements to other atomic and molecular ions (Ar^+, Kr^+, Xe^+, N_2^+, CO^+, Ar_2^+, Kr_2^+, and N_4^+) reacting with ethane, propane, and butane [56] and similar conclusions were reached. The observed increases in the fragment-ion yields with increasing collision energy were attributed to collision-induced excitation and dissociation of the product hydrocarbon ions. The transition from nondissociative to dissociative electron transfer has been scrutinized in a combined VT-SIFT and HTFA study of reactions of several atomic and molecular cations with benzene [43]. Attempts also were made to assign product-ion structures. A schematic reaction-coordinate diagram was constructed for the primary dissociation channels of $C_6H_6^+$ and the reaction pathway for production of $C_5H_3^+$ was discussed. Further, very

recent, SIFT studies probing the dynamics of electron transfer have been reported by Adams and co-workers [57]. Rate coefficients and product distributions were measured for dissociative electron-transfer reactions of CCl_4 and SF_6 with atomic and molecular ions having recombination energies between 6.4 and 24.5 eV. Comparisons are made with photoelectron spectroscopy, TPEPICO and PEPICO data.

The VT-SIFT technique can be used to probe internal and translational energy effects on the rate coefficient for electron transfer [58]. Such measurements have been completed for the reaction of CO_2^+ with O_2. At relatively low center-of-mass kinetic energies the rate coefficient is insensitive to temperature so that rotation and bending-vibrational modes do not determine reactivity. A temperature enhancement by as much as one order of magnitude has been observed at higher center-of-mass kinetic energies that is attributed to excitation of the stretching-vibrational modes.

Electron transfer to atomic and molecular ions was investigated in a comparative SIFT study at 300 K of reactions of Kr^+, Kr_2^+, Xe^+, and Xe_2^+ with a large variety of molecules including CO, O_2, HCl, CO_2, N_2O, H_2S, COS, NH_3, CH_4, C_2H_6, C_3H_8, C_2H_4, and C_2H_2 [59]. Whereas only electron transfer was observed in the reactions of the atomic ions Kr^+ and Xe^+, both electron transfer and inert gas-atom/reactant-molecule switching was observed in the molecular-ion reactions producing ions such as $KrCH_4^+$ and $XeC_2H_2^+$.

Thermal-energy electron-transfer rate coefficients for reactions involving doubly charged ions were measured with flow-tube mass spectrometer techniques as early as 1971 by the group in Boulder, CO [60]. The charge separation reactions

$$Ca^{2+} + NO \rightarrow Ca^+ + NO^+ \quad (6)$$

$$Mg^{2+} + X \rightarrow Mg^+ + X^+ \quad (7)$$

with X = Xe, NO, O_2, N_2O, CO, CO_2, SO_2, NO_2 and NH_3 were characterized and interpreted in terms of the Landau-Zener curve-crossing model with difficulties being noted. The Birmingham group continued these measurements and reported the results of detailed 300 K studies of the reactions of the ground-state doubly-charged rare-gas ions. Ne^{2+}, Ar^{2+}, Kr^{2+} and Xe^{2+} (^3P), and their metastable ions ($^1D_2$, $^1S_0$) with rare-gas atoms [61,62] and several molecules [62–64].

Electron-transfer reactions with buckminsterfullerene have been extensively explored in our laboratory using the SIFT technique [65]. Experiments have shown that an electron can be removed from C_{60} in the gas phase at room temperature by cations having a recombination energy greater than the first ionization energy of C_{60}, IE(C_{60}) = 7.64 ± 0.02 eV, and by metastable rare-gas atoms with an excitation energy greater than IE(C_{60}) in Penning or chemi-ionization reactions. Remarkably, He^+ and Ne^+ were observed to remove two electrons from C_{60} at thermal energies in a novel electron-transfer electron-detachment process, illustrated for He^+ in reaction (8) [66].

$$He^+ + C_{60} \rightarrow C_{60}^{2+} + e + He \quad (8)$$

This process also has been observed with naphthalene [67].

C_{60}^{n+} cations have been observed to remove electrons from neutral molecules with sufficiently low ionization energies [65]. With C_{60}^+ ($n = 1$) the threshold for electron transfer with molecules of different ionization energies is determined simply by its recombination energy (7.64 ± 0.02 eV). When $n>1$, the barrier arising from coulombic repulsion between the two charged product ions shifts the threshold to ionization energies lower than expected from simple exothermicity considerations. Thus the threshold for the occurrence of electron transfer to C_{60}^{2+} (RE = 11.36 ± 0.05 eV) has been determined to be at IE ≲ 9.58 eV [68], while that for electron transfer to C_{60}^{3+} (RE = 15.6 ± 0.5) has been shown to be at IE ≲ 11.2 eV [69]. Fig. 14 shows a shift in the threshold for electron transfer proceeding in competition with direct attachment. Triply charged C_{60}^{3+} cations also have been observed to abstract two electrons from corannulene and the PAHs anthracene, pyrene, and benzo[rst]pentaphene (see Fig. 15) [70]. These molecules have sufficiently low first and second ionization energies to make double-electron

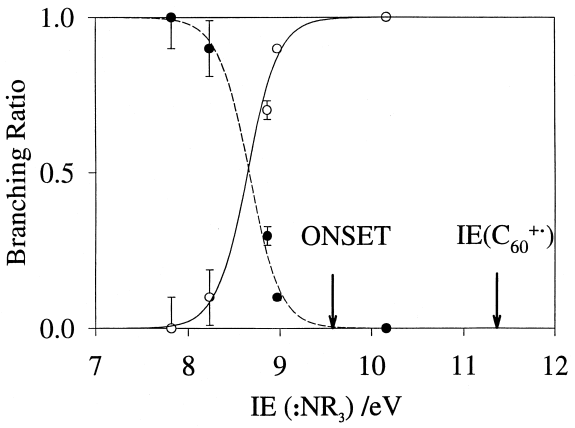

Fig. 14. Onset of electron transfer (dotted line) proceeding in competition with adduct formation (solid line) observed for reactions of C_{60}^{2+} with ammonia and amines in SIFT experiments at room temperature 294 ± 2 K and a helium pressure of 0.35 ± 0.01 Torr. The onset occurs at about 9.6 eV which is well below the recombination energy of C_{60}^{2+} (11.36 ± 0.05 eV).

transfer thermodynamically and kinetically favourable.

8. Proton transfer

The ease of generating protonated molecules in hydrogen carrier gas, particularly H_3^+ which has a relatively low proton affinity and is thus an effective proton donor in the flow tube, made the early FA technique ideally suited to measurements of the tendency for transfer of a proton between molecules. Early measurements with this technique by Burt et al. at York University surveyed the ability of H_3^+ to donate its proton to a large variety of molecules in reactions of type [71]

$$H_3^+ + X \rightarrow XH^+ + Y \quad (9)$$

and the preferred direction of proton transfer between molecules in reactions of type [72].

$$XH^+ + Y \rightleftarrows YH^+ + X \quad (10)$$

Rate coefficients, k_{10}, for many of these reactions were measured at room temperature and the judicious choice of X and Y allowed the measurements also of reverse rate coefficients, k_{-10}, and equilibrium constants, K_{10}, and so the standard free energy change $\Delta G°$ (10) [73]. Measurements as a function of temperature or calculations of the standard entropy change $\Delta S°$ (10) then allowed the evaluation of the standard enthalpy change $\Delta H°$ (10) and so the difference in the proton affinity PA(X) − PA(Y) [74]. The latter measurements provided scales of absolute proton affinities when referenced to a known proton affinity [75]. Proton affinities were reported for O_2, H_2, Kr, O, N_2, Xe, CO_2, CH_4, N_2O, and CO [75] as well as H_2O, H_2S, HCN, H_2CO, C_2H_4, and C_2H_6 [76,77]. It also became clear that proton transfer between these small molecules occurs rapidly with essentially unit probability when exoergic (see Fig. 16) [78].

The high (unit) efficiency of proton transfer allowed rate-coefficient measurements to be used for the systematic testing of classical ion–molecule collision rate theories as they were being developed in the seventies. Thus, survey measurements of rate coefficients for proton transfer with NH_3 [79], H_2O [80], HCN and CH_3CN [81], CH_3NO_2 [82], and H_2CO [83] provided tests for the Langevin, locked-dipole, average-dipole orientation and angular momentum-conserved average dipole orientation theories and measurements with C_2H_2 [84] provided a test for the average quadrupole orientation theory (see Fig. 17). Survey measurements have been reported for reactions of HCO^+, of special interest in interstellar and flame chemistry, and H_3O^+, of very broad interest in most areas of chemistry, with a variety of organic

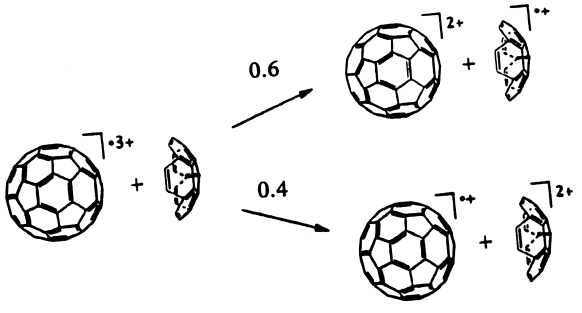

Fig. 15. Competition between single- and two-electron transfer observed between C_{60}^{3+} and corannulene [70].

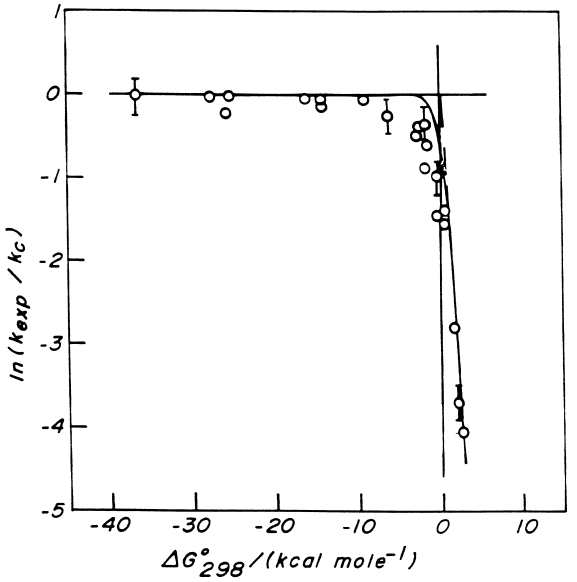

Fig. 16. Correlation between the efficiency of proton transfer, k_{exp}/k_c, and the overall change in standard free energy, $\Delta G°$, at 298 K [75]. The solid curve represents a model fit.

molecules. These also have been used to further test collision-rate theories including the Barker-Ridge theory [85,86] (see Fig 18).

Dissociative proton transfer may occur in sufficiently exothermic proton-transfer reactions as a consequence of the deposition of internal energy in the

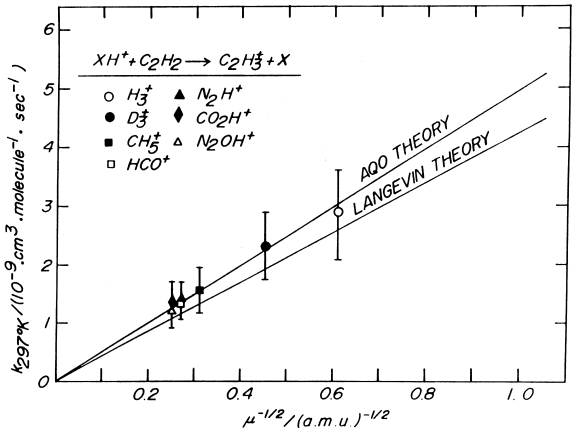

Fig. 17. A comparison of measured rate coefficients for proton transfer to acetylene with capture rate coefficients predicted by the Langevin and average quadrupole orientation theories [84]. The solid bars represent the estimated accuracy of the measurements.

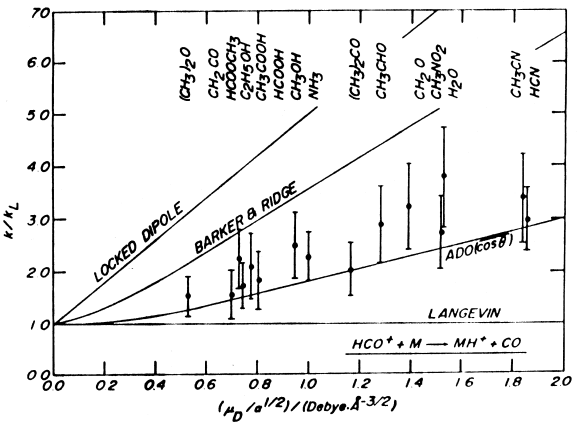

Fig. 18. A comparison of measured rate coefficients for proton transfer from HCO^+ to polar molecules with capture rate coefficients predicted by four different collision theories [85]. The solid bars represent the estimated accuracy of the measurements.

protonated product ion. This chemical activation can be controlled and its consequences monitored by choosing a variety of proton donors. For example, the following decomposition of nitromethane,

$$XH^+ + CH_3NO_2 \rightarrow [CH_3NO_2\,H^+]^* + X \qquad (11a)$$

$$[CH_3NO_2\,H^+]^* \rightarrow NO^+ + CH_3OH$$

$$\rightarrow CH_3NO^+ + OH \qquad (11b)$$

has been monitored in FA and SIFT experiments as a function of X over a difference in PA(X) of 80 kcal mol^{-1} [82]. Thus we have also reported systematic studies of the dissociative proton transfer to ethanol [85], formic and acetic acid [85–87], to several formate and acetate esters [88] and to ethane [89]. Such studies are of interest not only in chemical-ionization mass spectrometry but also in acid-catalyzed decompositions in solution.

Proton-transfer reactions of course are key to the success of chemical ionization mass spectrometry and therefore important in analytical chemistry. The practical application of flow-tube mass spectrometry to trace-gas analysis (see section 14) has led to a renewed interest in proton-transfer rate measurements and growth in the data base for rate coefficients and product-ion distributions involving a large variety of gases and vapours including alcohols, aldehydes,

ketones, carboxylic acids, esters, ethers, amines, organosulphur compounds, and hydrocarbons, and selected inorganic species of medical and environmental interest including NH_3, SO_2, NO, and NO_2 [90].

The occurrence of intramolecular proton transfer within reaction intermediates has been addressed by Henchman and colleagues in a study of H/D isotope exchange reactions in systems of the type XH_nH^+/XD_n (X=O, N, C) [91] and exemplified by

$$H_3O^+ + D_2O \rightarrow [H_3O^+ \ldots D_2O \rightleftarrows H_2O \ldots HD_2O^+ \rightleftarrows H_2DO^+ \ldots HDO] \rightarrow H_2DO^+ + HDO \quad (12)$$

Isotope exchange is the only possible consequence in intramolecular proton motion when X is atomic. For molecular X species, say AB, proton motion can lead to a change in the heavy-atom site of protonation and therefore can lead to catalyzed structural isomerization as illustrated by

$$ABH^+ + M \rightarrow [ABH^+ \ldots M \rightleftarrows AB \ldots HM^+ \rightleftarrows BA \ldots HM^+ \rightleftarrows BAH^+ \ldots M] \rightarrow BAH^+ + M \quad (13)$$

where M is a catalyst. A number of such isomerizations have been established experimentally using flow-tube mass spectrometry [92] and later treated theoretically as well [93–95]. Reaction (13) has been termed "proton-transfer catalysis" [90] and has found more general importance in the interpretation of ionic reaction mechanisms [96]. We also have identified an analogous mechanism for methyl cation transport [97].

Hydration/solvation can be brought about in flow-tube mass spectrometry either external to the flow tube or within the flow tube upstream of the reaction region and this allows the study of proton transfer as a function of hydration/solvation. We had reported in 1979 a systematic room-temperature FA study of the rates of reactions of NH_3, H_2S, and nine organic molecules with hydrated hydronium ions of type

$$H_3O^+ \cdot (H_2O)_n + B \rightarrow BH^+ \cdot (H_2O)_m + (n - m + 1)H_2O \quad (14)$$

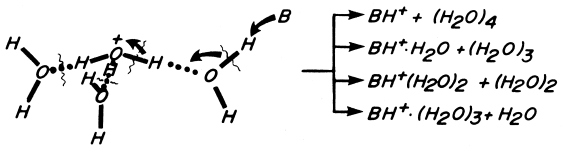

Fig. 19. Possible "proton-jump" mechanism for the gas-phase reaction of $H_3O^+.(H_2O)_3$ with B. The base B can attack at any edge of the hydrated hydronium ion and discretely pick up a proton along with one or more water molecules [78].

with *n* up to 3, where *m* may in principle have any value between 0 and *n* with the neutral water being released as individual molecules, dimers, or even polymers [98]. A structural interpretation proposed for reaction (14) is given in Fig. 19. Two extreme types of behaviour were reported for the influence of hydration on the reactivity of H_3O^+ (see Fig. 20): a slight or a precipitous decrease in reaction rate with increasing hydration [99,100]. These can be understood in terms of the preservation of exoergicity or a change in the sign of the reaction exoergicity. Hydra-

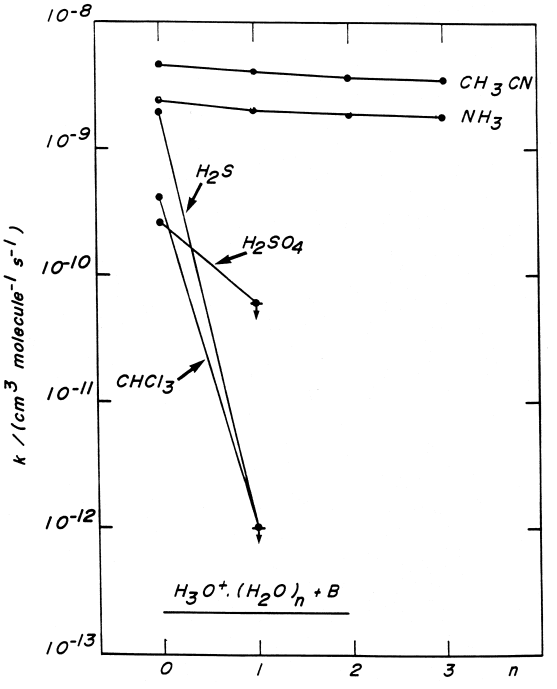

Fig. 20. Room temperature variation of the rate coefficient for reactions of hydrated hydronium ions with various molecules as a function of the number of hydrating water molecules.

tion in the case of formaldehyde leads to an equalization in the basicity of water and formaldehyde. However, because of the presence of water vapour in the flow tube, the product ion distributions for reaction (14) could not be unraveled. These early measurements have been superceded with improvements in techniques for the generation and introduction of hydrated and solvated ions into the flow tube that minimize or eliminate the presence of water vapour in the reaction region. A discussion of the results of these improved techniques will be continued in the section on atmospheric ion chemistry. Insight into the mechanism of reaction (14) has been provided by SIFT studies of H/D scrambling with B = NH_3 [101]. The discrete transfer of a proton together with the minimum number of water molecules that is energetically allowed is favoured over the formation of an intermediate complex that always decomposes by ejecting the maximum number of water molecules that is allowed.

Recently we also have explored proton transfer from multiply charged cations in our studies of the chemistry of derivatized fullerene dications [102] and trications [103] that indicated the occurrence of the following reactions at room temperature:

$$C_{60}(XH)_n^{2+} + XH \rightarrow C_{60}(XH)_{n-1}X^+ + XH_2^+ \quad (15)$$

$$C_{60}XH^{3+} + XH \rightarrow C_{60}X^{2+} + XH_2^+ \quad (16)$$

We have shown that for such reactions the "fast when exothermic" reactivity rule breaks down because of the "reverse activation energy" introduced by the coulombic repulsion between product ions. We have articulated this behaviour with the definition of an "apparent gas-phase acidity" that determines the occurrence or nonoccurrence of proton transfer involving multiply charged ions. Also, we have shown how taking into account coulombic repulsion can provide a quantitative determination of the gas-phase acidity GA ($C_{60}H^{2+}$) from bracketing reactivity measurements with $C_{60}H^{2+}$ [104]. Our model for the energetics of proton transfer from multiply charged fullerene ions applies generally to proton transfer involving multiply charged ions including multiply protonated peptides and proteins and indeed has been adopted in that field.

Before concluding this section on proton transfer it is worth also noting the remarkable observation in our laboratory of a proton elimination reaction proceeding at room temperature. We have found that the very high enthalpy of formation of C_{60}^{3+} can lead to the exothermic heterolytic dissociation of hydrogen halide molecules in reactions with X = Cl and Br [105] of type

$$C_{60}^{3+} + XH \rightarrow C_{60}X^{2+} + H^+ \quad (17)$$

9. Ion–ion and ion–electron recombination

The development of the FALP technique has allowed the systematic study of a wide variety of plasma reaction processes over the wide temperature range from ~80–600 K [106]. These studies have been carried out by David Smith and Nigel Adams at Birmingham and later by Adams in Georgia. Both positive ion–negative ion recombination and positive ion–electron recombination have been investigated. Ion–ion recombination measurements are possible when the FA plasma is converted entirely to an ion–ion plasma: the decay rates of the positive and negative–ion densities can be measured and hence the ion–ion recombination (mutual neutralization) rate coefficients can be obtained. A large number of ion–ion recombination rate coefficients have been measured at thermal energies involving a variety of ions, including many "cluster" positive and negative ions such as $H_3O^+(H_2O)_3$ and $NO_3^-(HNO_3)$. These data are important in the calculation of de-ionization rates in the terrestrial stratosphere and troposphere. Also, the neutral products of the $NO^+ + NO_2^-$ reaction were determined using emission spectroscopy studies which have recently been extended to include the reactions of NO^+ with Cl^- and I^-.

The greater versatility of the flowing afterglow method, compared to the stationary afterglow/microwave cavity method that previously had provided basic data on dissociative recombination at thermal energies, offered the opportunity to extend the mea-

surements of dissociative recombination coefficients to a much greater number of positive-ion species. Thus the dissociative recombination coefficients for many ions, including the ionospherically important species O_2^+ and NO^+ and the interstellar ions, HCO^+, N_2H^+, H_2CN^+, and H_3O^+, have been determined, some over the temperature range from 80 to 600 K [107]. A major, important discovery has been that H_3^+ ions recombine only very slowly with electrons, a result that has significant implications to interstellar physics and chemistry but is still controversial [108]. More recent developments have allowed the determination of the dissociative recombination coefficients for some reactions at elevated T_e (up to ~3000 K) which has obvious relevance to the thermospheric plasma. This has required the development of the Langmuir probe technique to determine electron energy distributions in these decaying plasmas and the use of argon carrier gas to obtain high T_e ($>T_g$) in the afterglow.

Also, using the FALP, the first-ever studies of some of the neutral products of the dissociative recombination of several interstellar species including H_3O^+, HCO_2^+, CH_5^+, O_2H^+, N_2H^+, and N_2OH^+, have been determined by applying laser-induced fluorescence (LIF) and visible–ultraviolet spectroscopic diagnostic techniques to the recombining FALP plasmas [109–114]. The use of the flowing afterglow for studies of rate coefficients and products of dissociative electron–ion recombination using Langmuir probes and optical spectroscopy has been reviewed by Nigel Adams [115]. This technique has become quite sophisticated. For example, the effects of deuteration on vibrational excitation in the products of the electron recombination of HCO^+ and N_2H^+ have been examined in a very recent application [112] (see Fig. 21).

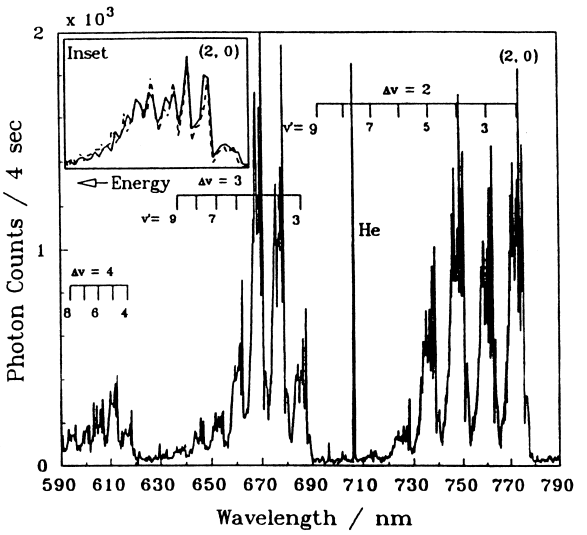

Fig. 21. Medium resolution spectra of N_2 ($B\,^3\Pi_g \rightarrow A\,^3\Sigma_u^+$) emissions resulting from the dissociative electron recombination of and N_2D^+ [112]. The inset shows the (2,0) emission band expanded (solid line) along the abscissa with wavelength converted to cm^{-1} and overlaid by a synthetic spectrum for the (1,0) band generated for a rotational temperature of 400 K (dashed curve).

10. Metal and organometallic ion chemistry

The early flow-tube studies of metal-ion chemistry by Fehsenfeld, Ferguson, and co-workers, the first of their kind, were directed to metals such as lithium [116], magnesium [117,118], sodium [119], calcium [118], barium [118], and silicon [120] that are deposited in the atmosphere by meteor ablation. Both singly charged atomic and atomic-oxide ions and doubly charged atomic ions were produced either in situ in the FA configuration or prior to selection in the SIFT configuration and their reactions were investigated with common atmospheric gases. These measurements established some important fundamental features for the chemical kinetics of metal ions. Termolecular kinetics was established for the association reactions of Li^+ with N_2, CO_2, SO_2, halogenated methanes, and halogenated ethylenes with measurements over a pressure range from 0.3 to 1.0 Torr. Saturated termolecular association was observed with the larger molecules C_4F_8, $C_2Cl_2F_4$, and C_2F_6. Bimolecular oxide and hydroxide formation (followed by hydration) was observed for several reactions with Mg^+, whereas N_2O was found to be an effective O-atom donor for Ba^+ and Ca^+. In contrast Na^+ chemistry was dominated by association and switching reactions with the molecules chosen for study.

Association reactions were observed for the first time with the doubly charged ions Mg^{2+}, Ca^{2+}, and

Ba^{2+} and multiple sequential ligation (up to six) was observed with O_2, N_2, and CO_2 [118]. The rate coefficients for ligation were found to be up to 500 times higher than for those of singly charged ions and equilibrium measurements provided some of the smaller ligation energies. The measured rate coefficients were correlated with the ionic radii of the doubly charged ions and the ligation energy. Charge-separation reactions were reported for the first time for several reactions of Mg^{2+} and the reaction of Ba^{2+} with NO [121]. A curve-crossing model was applied to these electron-transfer reactions and Landau-Zener calculations were used to deduce electron-transfer efficiencies at thermal energies.

Results of reactions of selected alkali-metal ion adducts with selected atmospheric molecules led Ferguson and co-workers to first propose the notion of ion catalysis in the gas phase [122]. For example, the rate of the reaction of O_3 with NO to produce NO_2 and O_2 was found to be enhanced by up to a factor of 10^6 when mediated by an atomic alkali cation as in

$$X^+ \cdot O_3 + NO \rightarrow X^+ + NO_2 + O_2 \qquad (18)$$

for X = Li, Na, and K. Analogous results were observed for the reaction of N_2O_5 with NO, the reaction of O_3 with CO and the reaction of SO_2 with O_3 with the first reagent attached to the alkali ion in each case. The reaction exothermicity can be large enough to release the product neutrals from the metal ion. Activation energies for neutral reactions of more than 28 kcal mol^{-1} apparently can be overcome in this way as reported in a follow-up study by Viggiano et al. [123] who observed rate enhancements of up to 30 orders of magnitude for the reaction of NO_2 with CO to produce CO_2 and NO in the presence of Li^+ or Na^+! In explanation, these authors have discussed a model for the potential-energy surface of ion-catalyzed reactions in which the electrostatic energy of interaction between the alkali ion and the neutral reactant has a rate-determining influence.

Flow-tube mass spectrometry also is ideally suited for the characterization of intrinsic features of the ligation of organometallic ions at room temperature and so to explore fundamental aspects of this important process in solution. Unligated and ligated ions may be produced within the ion source or upstream of the reaction region before allowing further ligation downstream according to reactions of type

$$ML_n^+ + L + He \rightarrow ML_{n+1}^+ + He \qquad (19)$$

The helium bath gas is sufficiently high in pressure to bring about collisional stabilization of the ligated product ion. Measurements of rate coefficients for sequential ligation reactions of type (19) provide insight into the intrinsic efficiency of ligation. They also provide a kinetic measure of the intrinsic coordination number of the core ion since the rate coefficient for ligation is sensitive to the bond energies of the ligated ion, $D(ML_n^+\text{-}L)$. This is because gas-phase ligation at moderate pressures proceeds through the formation of a transient intermediate with a lifetime against back dissociation that depends both on the degrees of freedom effective in intramolecular energy redisposition in the transient intermediate $(ML_{n+1}^+)^*$ and on its attractive well depth, $D(ML_n^+\text{-}L)$, viz. the ligation energy of ML_n^+. When the ligand is capable of hydrogen bonding as is the case with water and ammonia, for example, two types of ligation can occur: the ligand either can bond directly to the core ion ("inner-shell" ligation) or it may bond to an existing ligand by weak hydrogen bonding ("outer-shell" ligation). The difference in ligation energy between inner-shell ligation and outer-shell ligation in principle can be detected with CID measurements and also can lead to a measurable difference in the rate coefficient for ligation and so allow an identification of the occurrence of a transition between inner-shell and outer-shell ligation.

In our laboratory the ligation studies are augmented by subjecting the ligated ions produced in reaction (19) to multicollision induced dissociation and measuring their dissociation thresholds. Such measurements provide relative binding energies and insights into the occurrence of intramolecular ligand–ligand interactions by revealing bond connectivities in the ligated ions. Standard free energies of ligation become accessible when they are sufficiently small ($<\sim$10 kcal mol^{-1} at room temperature) for the

ligation reaction to achieve equilibrium. Also relative M^+-L ligand-bond energies can be deduced from kinetic measurements by establishing the preferred directions of ligand-switching reactions of type

$$ML'^+ + L'' \rightarrow ML''^+ + L' \quad (20)$$

or by measuring the rate coefficient for ligation in both directions. The use of kinetic measurements for establishing relative Fe^+-L ligand-bond energies in ligand-switching reactions of type (20) has been illustrated in the laboratory of Chava Lifshitz [124]. $Fe(CS_2)^+$ was produced from the reaction of $FeCO^+$ with CS_2 (either in the ion source or upstream of a SIFT apparatus) and systematically reacted with a variety of organic ligands and ammonia. The onset of the switching reaction provided a measure of $D(Fe^+$-$CS_2)$ from the known ligation energies of Fe^+ with the ligands investigated.

Ground-breaking measurements of metal–cation ligation kinetics were reported by Castleman and co-workers in the late 1980s. Termolecular association kinetics was established for the ligation of Ag^+ and Cu^+ (produced by thermionic emission) with CO, CH_4, CH_3F, CH_3Cl, and CH_3Br [125]. More extensive measurements as a function of temperature were reported for the ligation of Na^+ with HCl, CO_2, NH_3, ND_3, SO_2, and CH_3OH [126] and then room temperature measurements of association reactions with H_2O, NH_3, CH_3OH, CH_3CN, CH_3CHO, CHsCOOH, CH_3COCH_3, CH_3COOCH_3, and $CH_3OC_2H_4OCH_3$ and bimolecular switching reactions of the first three members of this series with the remaining molecules [127]. Also room-temperature ligation kinetics was reported for Bi^+ and Pb^+ with NH_3, O_2, CH_3Cl, CH_3OH, CH_3SH, and CH_3NH_2 [128].

Water and methanol were investigated as ligands in the solvation of Mg^+ and the alkali metal ions Li^+, Na^+, K^+, Rb^+, and Cs^+, respectively [129,130]. Dehydrogenation reactions of type

$$Mg^+(H_2O)_n^+ + H_2O \rightarrow MgOH^+(H_2O)_n + H \quad (21)$$

for $n > 4$, similar to those observed with protonated methanol clusters, were observed at specific degrees of ligation with a small dependence on the size of the core ion. Observations of magic numbered $Cs^+(H_2O)_n$ clusters with $n = 18$, 20, 24, 27, and 29 has led to the proposal of the remarkable formation of ionic clathrates through intramolecular ligand interactions mediated by Cs^+ and leading to its encagement [131]. Several proposed structures are shown in Fig. 22.

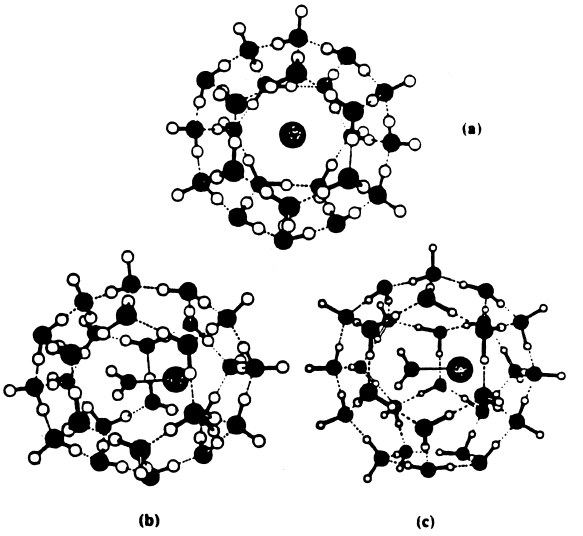

Fig. 22. Proposed structures for (a) $Cs^+(H_2O)_{24}$ (12 pentagons and 2 hexagons), (b) $Cs^+(H_2O)_{27}$ (12 pentagons and 3 hexagons), and (c) $Cs^+(H_2O)_{29}$ (12 pentagons and 4 hexagons) [131]. The two larger clusters contain the Cs^+H_2O ion.

Weisshaar and co-workers, using an excimer laser for in situ laser ablation/ionization of rotating metal disks in helium bath gas at 1 Torr, have tracked across the periodic table the intriguing reactivity patterns of the transition metal ions Sc^+, Ti^+, V^+, Cr^+, Mn^+ Fe^+, Co^+, Ni^+, Cu^+, and Zn^+ with the small alkanes methane, ethane, and propane [132]. The observed chemistry was dominated by ligation although elimination channels were observed to compete in a number of cases. The measured rate coefficients varied widely and nonmonotonically across the transition metal series and the variation is remarkably similar for the three alkanes (see Fig. 23). A qualitative model was presented that includes the interplay of metal-ion size effects on long-range repulsive forces, of poten-

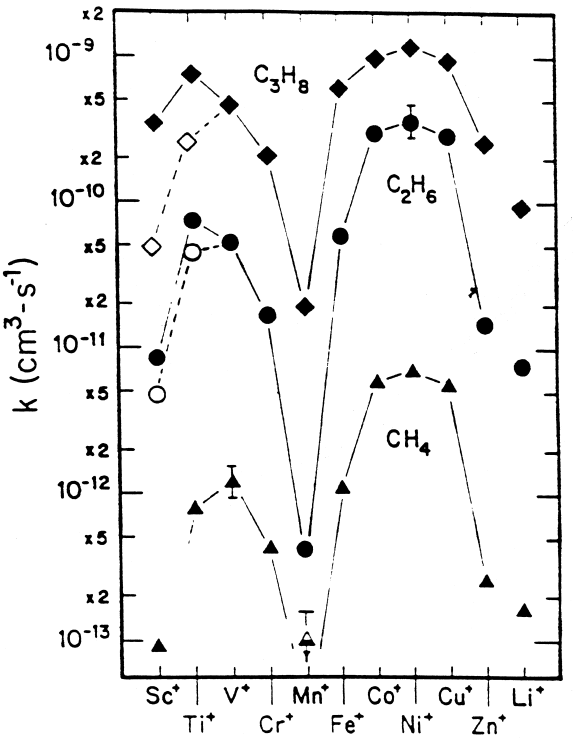

Fig. 23. Variation in the effective bimolecular rate coefficient for reactions of transition-metal ions with alkanes at 300 K and 0.75 Torr of He. The open points are rate coefficients with the effect of elimination subtracted out [132].

tial-energy surface crossings, and of orbital symmetry and electron-spin conservation.

Other ligation studies using still other sources for metal ions have been reported. For example, the ligation of Co^+, Ni^+, Cu^+, and Zn^+ with ethane was investigated in a FA study using a sputtering-glow discharge as a source of transition metal ions [133]. The availability of the newly constructed ICP/SIFT/CID apparatus in our laboratory will increase the scope of such atomic–ion ligation measurements enormously as essentially any atomic ion on the periodic table can be injected into the flow tube, ligated by bimolecular or termolecular reaction upstream of the reaction region and then exposed to further ligation reactions downstream.

Our pre-2000 studies of ion ligation were focused on the ligation of FeO^+ (produced either within the source or upstream in the flow tube from the reaction of Fe^+ with N_2O) [134–136], Fe^+ [134,137–139], (c-C_5H_5)Fe^+, and (c-C_5H_5)$_2Fe^+$ cations (produced from the electron-impact ionization of ferrocene) [135,138,139] as well as Mg^+ [138,140,141], (c-C_5H_5)Mg^+ and (c-C_5H_5)$_2Mg^+$ cations (produced from magnesocene) [140,141]. Indications are that the ions produced in this fashion are predominantly in their ground electronic state. The survey of the intrinsic coordination kinetics of FeO^+, bare Fe^+ and Mg^+, and the influence of one and two c-C_5H_5 substituents on the kinetics of the latter two, was relatively straightforward and has been achieved with the inorganic ligands H_2, HD, D_2, NH_3, H_2O, N_2, CO, NO, O_2, CO_2, NO_2, and N_2O and a variety of organic ligands including saturated and unsaturated hydrocarbons. The kinetics of ligation also has been followed as a function of the size and number of ligands and coordination numbers to the core metal ions have been assigned accordingly. Bond connectivities and relative ligation energies were explored concomitantly by multicollision induced dissociation. Some of the important findings so far are the following.

Our results for the systematic studies of the single ligation of Mg^+, (c-C_5H_5)Mg^+ and (c-C_5H_5)$_2Mg^+$ with homologous alkanes are illustrative of the dependence of the rate of ligation on the size (degrees of freedom) of the ligand (see Fig. 24) and the role of c-C_5H_5 substituents on the efficiency of Mg ligation (see Fig. 25) [141]. Correlations of measured thresholds for multicollision induced dissociation of ligated Mg^+ and (c-C_5H_5)Mg^+ with the polarizabilities of the alkane ligands have provided insights into the electrostatic nature of ligand bonding.

Sequential ligation reactions that lead to the formation of multiply ligated ions have been observed with many ligands. This, of course, is somewhat akin to multiple solvation. When a ligand has the ability to hydrogen bond a transition may occur from inner-shell ligation in which the ligand bonds directly with the core ion to outer-shell ligation in which the ligand attaches by hydrogen bonding to an existing inner-shell ligand.

The approach is illustrated in Figs. 26 and 27 for the ligation of Fe^+ and (c-C_5H_5)Mg^+ with ammonia

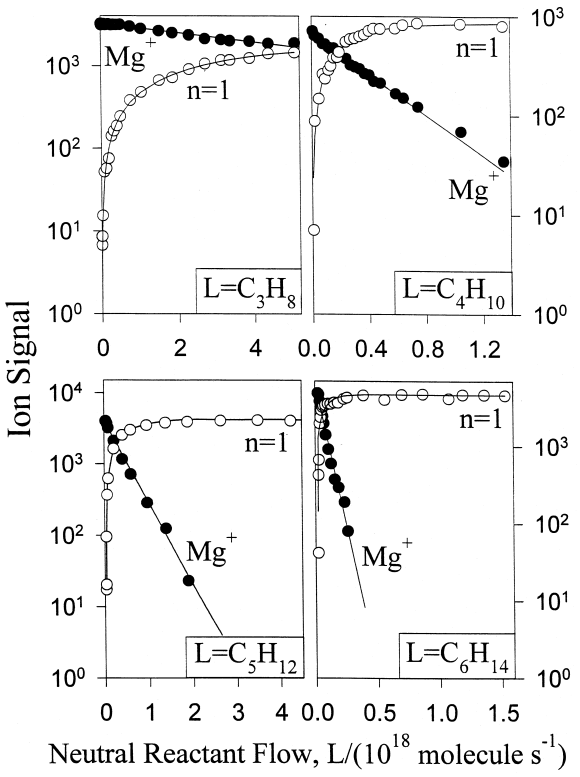

Fig. 24. Composite of kinetic data obtained for reactions of Mg^+ to produce MgL_n^+ with L = *n*-propane, *n*-butane, *n*-pentane, and *n*-hexane [141]. The measurements were performed at 294 ± 3 K and at a helium buffer-gas pressure of 0.35 ± 0.01 Torr. The solid lines represent a computer fit of the experimental data with the solution of the appropriate differential equations.

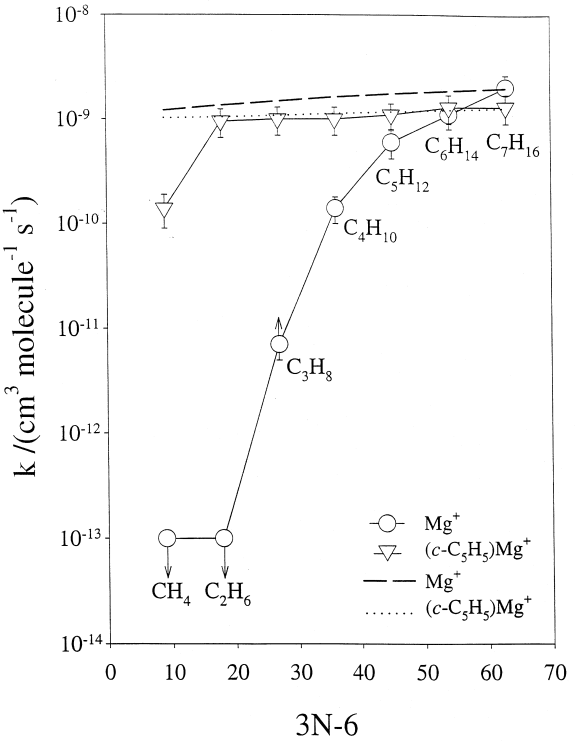

Fig. 25. Variation of the effective bimolecular rate coefficient of ligation with the degrees of freedom $3N-6$ of the ligand (*N* is the number of atoms) [141]. The measurements were performed at (294 ± 3) K and at a helium buffer-gas pressure of (0.35 ± 0.01) Torr. The dashed and dotted lines represent the variation of the calculated collision rate coefficient.

[138]. The rapid ligation of Fe^+ with two molecules of ammonia, followed by a much slower third addition, and the much lower onset energy for the multi-collisional dissociation of the third ligand compared with the first two, can be interpreted in terms of a primary coordination number of two with a third ammonia molecule weakly hydrogen bonding in an outer shell. Fig. 27 shows the rapid ligation of three molecules of ammonia to $(c\text{-}C_5H_5)Mg^+$ that is representative of a total coordination number of four for this ion. The CID profiles are consistent with this interpretation but it is interesting to note that the CID profile of $(c\text{-}C_5H_5)Mg(NH_3)_3^+$ shows two populations that imply the occurrence of hydrogen bonding of the third ammonia ligand in a fraction of the $(c\text{-}C_5H_5)Mg(NH_3)_3^+$ ions. Fig. 28 provides an overview of the coordination kinetics of $(c\text{-}C_5H_5)Mg^+$ with inorganic ligands. Noteworthy is the apparent high coordination number with water that has been interpreted in terms of a primary coordination number of 3 and hydrogen bonding in an outer ligation/solvation shell.

With unsaturated hydrocarbon ligands we have observed the Fe^+ mediation of intramolecular ligand–ligand interactions [137]. The CID results have provided evidence for the occurrence of intramolecular interactions between ligands mediated by Fe^+ resulting in C–C bond formation in the ligated ions $Fe(1,3\text{-}C_4H_6)_4^+$, $Fe(C_2H_2)_3^+$ and $Fe(C_2H_2)_5^+$, $Fe(CH_3C_2H)_2^+$ and $Fe(CH_3C_2H)_4^+$ and $Fe(C_4H_2)_2^+$

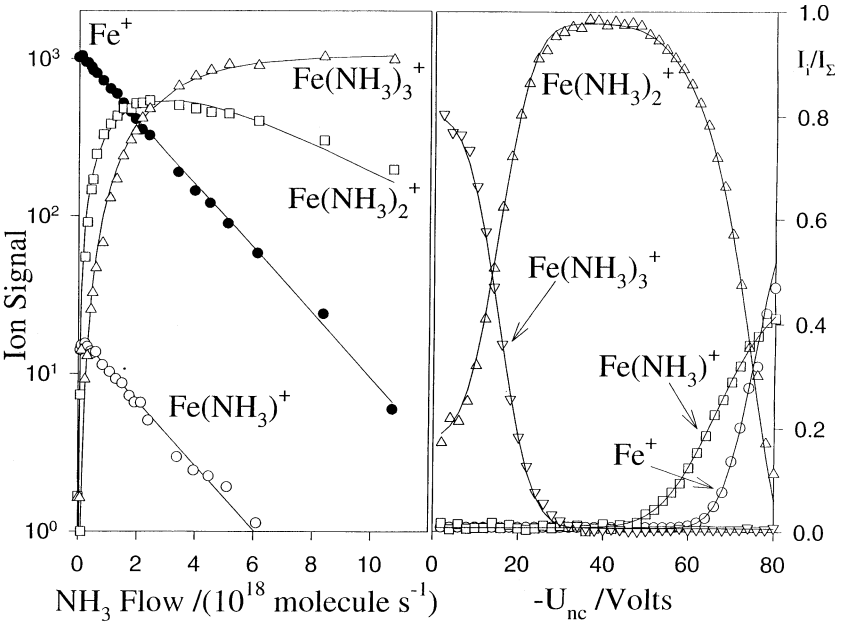

Fig. 26. (Left) SIFT data recorded for the reaction of Fe^+ with ammonia in helium buffer gas at 294 ± 3 K and 0.35 ± 0.01 Torr [138]. The Fe^+ ions were produced in a low-pressure ion source by electron impact dissociative ionization of ferrocene vapour at 35 eV. The solid lines represent a fit to the experimental data with the solution to the differential equations appropriate for the sequential addition reactions. (Right) Results of multicollision CID experiments [138]. The flow of ammonia is 1.3×10^{19} molecules s^{-1}.

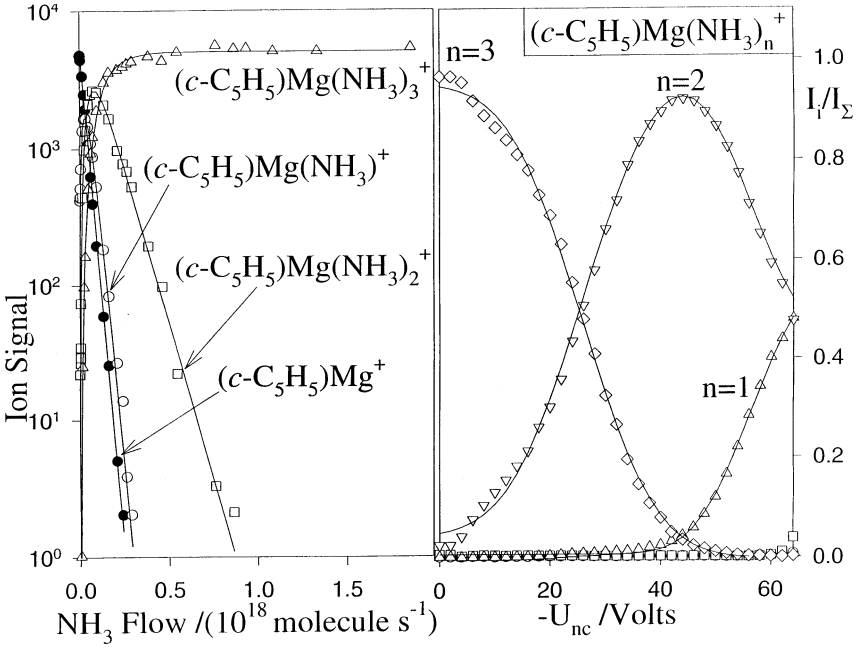

Fig. 27. (Left) SIFT data recorded for the reaction of $(c\text{-}C_5H_5)Mg^+$ with ammonia in helium buffer gas at 294 ± 3 K and 0.35 ± 0.01 Torr [138]. The $(c\text{-}C_5H_5)Mg^+$ ions were produced in a low-pressure ion source by electron impact dissociative ionization of magnesocene vapour at 50 eV. The solid lines represent a fit to the experimental data with the solution to the differential equations appropriate for the sequential addition reactions. (Right) Results of multicollision CID experiments. The flow of ammonia is 1.0×10^{18} molecules s^{-1}.

and $Fe(C_4H_2)_4^+$. The postulated interligand interactions are attributed to cyclization or oligomerization reactions leading to the formation of benzene (see Fig. 7), dimethyl- and diethynyl-cyclobutadiene in $Fe(C_2H_2)_3^+$, $Fe(CH_3C_2H)_2^+$ and $Fe(C_4H_2)_2^+$, respectively, and the formation of a dimer of 1,3-butadiene in $Fe(1,3\text{-}C_4H_6)_4^+$.

We have also extended our ligation studies to other, larger carbonaceous ligands, some large enough to mimic surfaces in the gas phase. This is possible with a flow-tube mass spectrometer because any ion may, in principle, be selectively ligated upstream in the flow tube by termolecular addition to the vapour of a ligand before being further reacted or ligated downstream in the reaction region. We began our studies of "gas-phase surface chemistry" by investigating the chemistry of Si^+ attached to benzene or naphthalene with D_2, CO, N_2, O_2, H_2O, NH_3, C_2H_2, and C_4H_2 [142,143]. New reaction paths were observed with Si^+ attached to these aromatic molecules compared to free Si^+ ions. Trapping on polycyclic aromatic hydrocarbons is thought to be a major loss process for atomic metal ions in the interstellar medium because of their inefficient recombination with electrons. More recently we have extended these studies to Fe^+ attached to coronene, corannulene and C_{60}. The reactions of Fe^+ coordinated to the π-donating ligands C_2H_4, *c*-C_5H_5, C_6H_6, and C_{60} with N_2O and CO were examined first in a comparative study designed to probe the nature of the bonding in $C_{60}Fe^+$ [144]. Fig. 29 shows the match in reactivity with N_2O found when Fe^+ is attached to C_2H_4 and C_{60} and this suggests η^2 coordination of Fe^+ to C_{60}. Both react according to

$$XFe^+ + N_2O \rightarrow XFeO^+ + N_2 \quad (22a)$$

$$\rightarrow XFe(N_2O)^+ \quad (22b)$$

with similar overall rate coefficients but different branching ratios. Now we are systematically investigating reactions of Fe^+ attached to various carbon networks with different curvature: corannulene, coronene and C_{60} and probing the influence of curvature on this gas-phase surface chemistry.

Finally, the chemistry of pure metal-cluster ions also can be measured with flow-tube mass spectrometry. For example, reactions of pure metal-cluster cations (Cu_n^+, $n = 1$–14) have been produced in a laser vapourization/FA apparatus and their association rate coefficients have been measured with CO [145]. Termolecular kinetics was seen for low cluster sizes ($n<8$) but rate coefficients became pressure independent for higher cluster sizes at buffer-gas pressures >0.3 Torr.

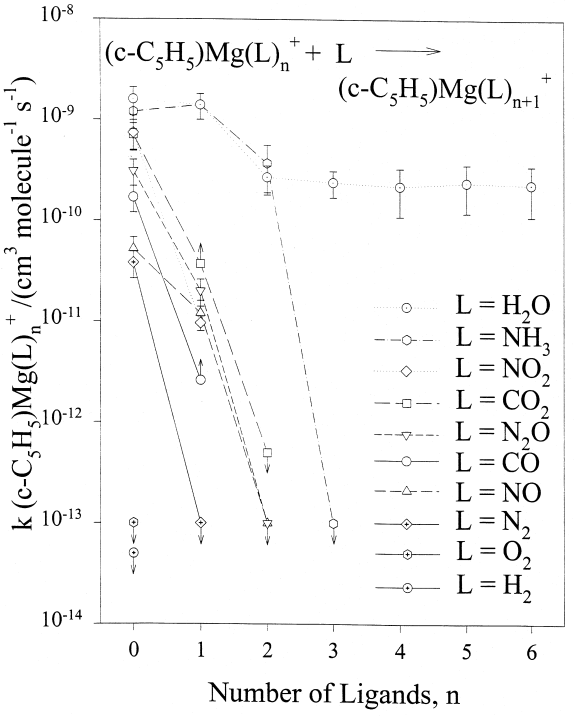

Fig. 28. A semilogarithmic correlation of the rate coefficient for the sequential ligation of (*c*-C_5H_5)Mg^+ by a variety of inorganic ligands as a function of the number of ligands, *n*, added in the gas phase at (294 ± 3) K and at a helium buffer-gas pressure of (0.35 ± 0.01) Torr [140].

11. Fullerene–ion chemistry: chemistry as a function of charge state

At York University we have found the SIFT apparatus to be ideally suited to the study of the chemistry of fullerene ions and of ions with neutral fullerenes. Buckminsterfullerene, C_{60}, is readily vapourized and ionized to its first three charge states

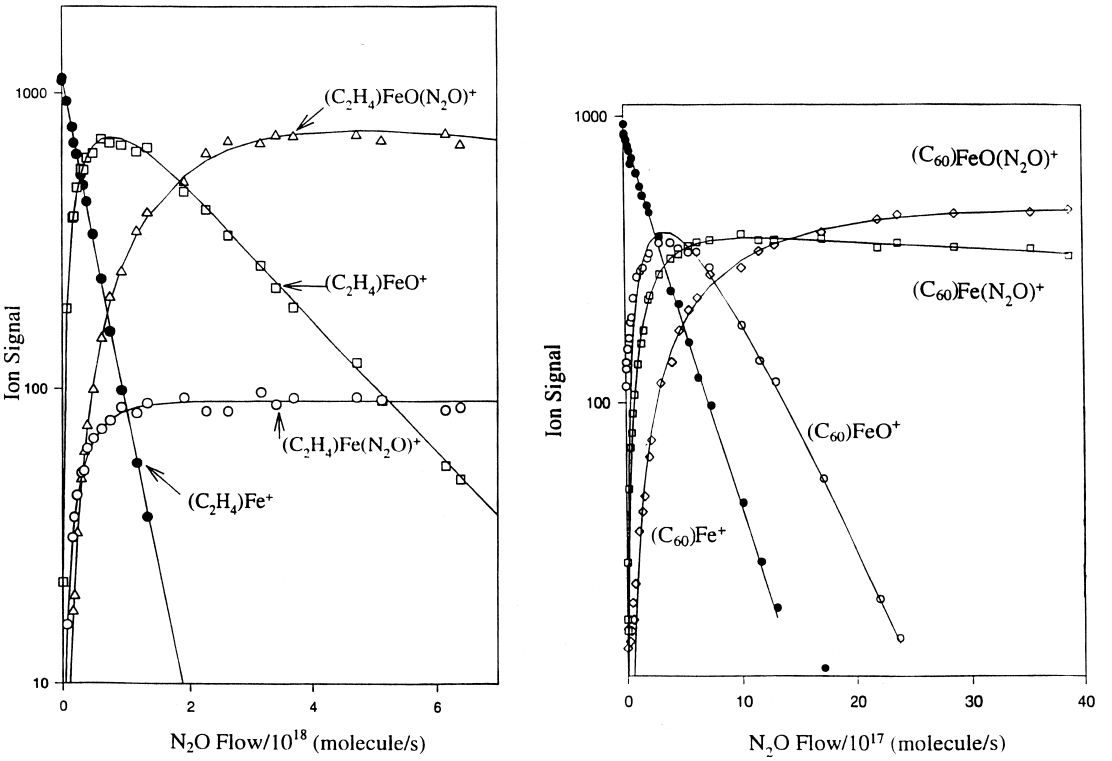

Fig. 29. Experimental data for the reactions of $(C_2H_4)Fe^+$ (left) and $C_{60}Fe^+$ with N_2O [145]. The solid lines represent fits to the data with the solutions of the systems of differential equations appropriate for the observed sequential reactions.

using conventional electron-impact techniques. Selection of the appropriate charge state then allowed the systematic SIFT investigation of fullerene cation chemistry as a function of charge state. Our measurements of the rates and products of chemical reactions of fullerene cations in the gas phase began in 1990, immediately after C_{60} samples became available for the first time. These measurements showed that fullerene carbocations are extensively reactive, dramatically so as the charge state increases, and that new chemical pathways become accessible as the charge state increases from 1 to 2 to 3 [146]. Both bond-redisposition and charge-separation reactions occur with these higher charge states. The following reaction summarizes the various types of reactive encounters that were identified with the more than 30 different molecules that have been surveyed:

$$C_{60}^{n+} + XY \rightarrow C_{60}XY^{n+} \quad (23a)$$

$$\rightarrow C_{60}X^{n+} + Y \quad (23b)$$

$$\rightarrow C_{60}X^{(n-1)+} + Y^+ \quad (23c)$$

$$\rightarrow C_{60}^{(n-1)+} + XY^+ \quad (23d)$$

$$\rightarrow C_{60}^{(n-1)+} + X^+ + Y \quad (23e)$$

$$\rightarrow C_{60}^{(n-2)+} + XY^{2+} \quad (23f)$$

These types include attachment, (23a), dissociative attachment, (23b), dissociative attachment with charge separation, (23c), single-electron transfer, (23d), dissociative single-electron transfer, (23e), and two-electron transfer, (23f), respectively. The most extreme behaviour observed with a particular reactant molecule ranges from no observable reaction with singly charged C_{60} (C_{60}^+), $k < 5 \times 10^{-14}$ $cm^3\,molecule^{-1}\,s^{-1}$, to very rapid dissociative electron transfer with triply charged C_{60} (C_{60}^{3+}), $k > 10^{-9}$

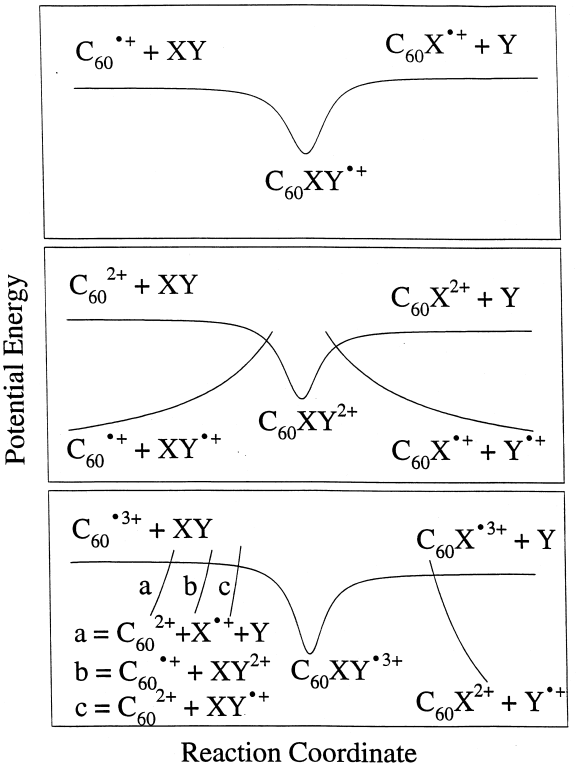

Fig. 30. Summary of plausible potential-energy profiles for reactions (22a)–(22f) as a function of charge state [148]. Bonding reactions are described in terms of attractive potential-energy profiles, which, for dissociative attachment leading to charge separation, are intersected by repulsive curves. Nonbonding reactions involving electron transfer that lead to charge separation are also described in terms of repulsive potential-energy profiles.

cm^3 $molecule^{-1}$ s^{-1}. Fig. 30 provides plausible potential-energy profiles computed for reactions (23a)–(23f) using standard r^{-4} and r^{-6} attractive potentials and r^{-12}, and r^{-1} (coulombic) repulsive potentials [147,148]. These profiles allow a qualitative rationalization of the remarkable changes in reaction type and rate observed for reactions involving the first three charge states of C_{60} cations. Direct and, to a lesser extent, dissociative attachment leading to chemical-bond formation with C_{60} is a common feature of the reactions of the first three charge states of C_{60} but, as the charge state increases from 1 to 2 and 3, other, bimolecular, reactions begin to compete. Perhaps not surprisingly, electron transfer becomes increasingly important with increasing electron recombination energy of the fullerene cation, often being dissociative with C_{60}^{3+}.

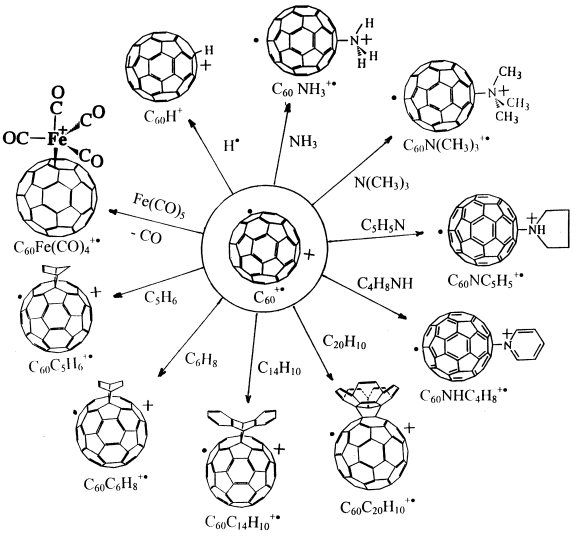

Fig. 31. An overview of derivatization reactions of C_{60}^+ observed with the York University SIFT apparatus at room temperature in helium buffer gas at 0.35 Torr. The assigned structures are speculative.

C_{60}^+ has been observed to be quite unreactive toward many molecules in helium buffer gas at 0.35 Torr. The important exceptions [146] are shown in Fig. 31 which indicates that C_{60}^+ has been seen to bond to H atoms, to strong nucleophiles containing nitrogen such as ammonia, saturated amines, pyrrolidine [149] and pyridine [150], and to molecules capable of Diels-Alder addition. The reaction of C_{60}^+ with iron pentacarbonyl is the only example of a bimolecular derivatization reaction reported to date [151]. The difficulty in covalent bonding to C_{60}^+ has been attributed to the distortion of the C_{60} carbon cage required at the C site of bond formation with the substituent so as to achieve sp^3 hybridization. C_{60}^{2+} has been observed generally to be easier to derivatize than C_{60}^+. This enhanced reactivity has been attributed to the stronger electrostatic interaction between molecules and C_{60}^{2+} that may serve to overcome the activation barrier associated with the change in hybridization required at the site of bonding. Fig. 32 indicates derivatization reactions observed with C_{60}^{2+}. With chlorinated ethylenes (not included in Fig. 32)

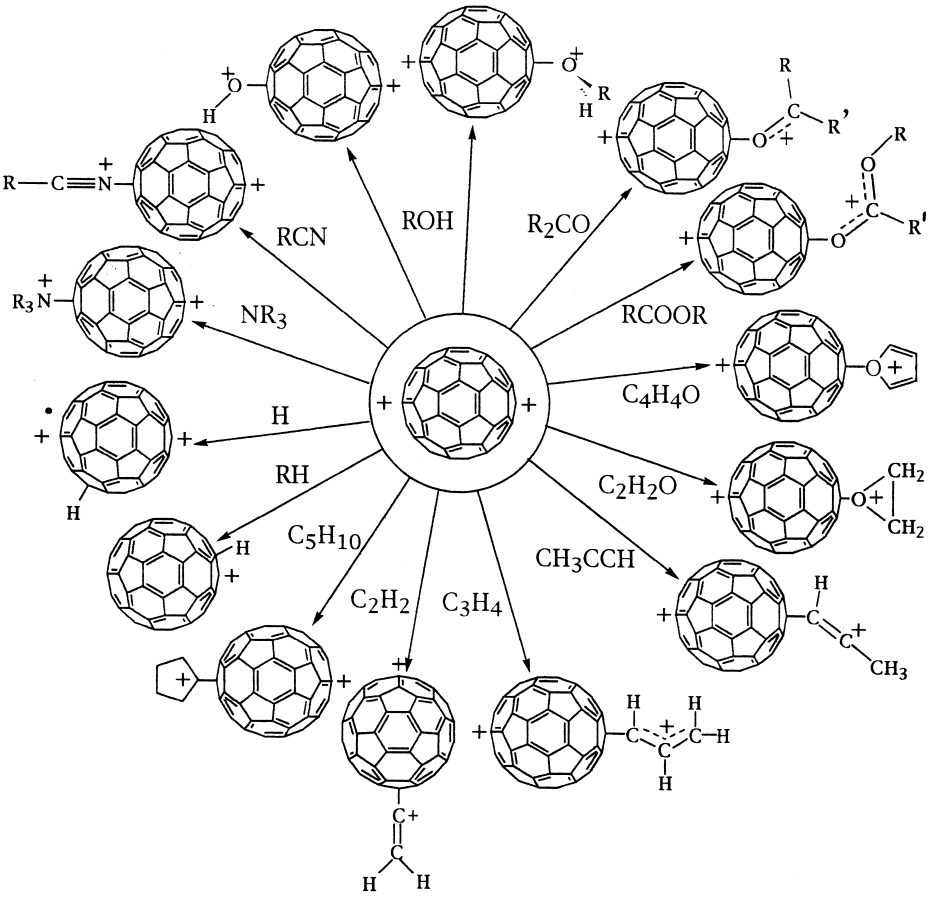

Fig. 32. An overview of derivatization reactions of C_{60}^{2+} observed with the York University SIFT apparatus at room temperature in helium buffer gas at 0.35 Torr [146]. The assigned structures are speculative.

[152], C_{60}^{2+} exhibited three different types of reaction channels: electron transfer, adduct formation and $(Cl)_2$ transfer. The latter channel was the only chlorination channel observed and, curiously, occurred exclusively with the cis and trans isomers of 1,2-dichloroethylene, but in competition with adduct formation. The variation observed in the occurrence of these three channels with charge state is consistent with what is now known about the role of charge state in promoting bond formation with the C_{60} surface and the role of coulombic repulsion between product ions in preventing electron transfer [152].

Electron transfer is an important competitive channel for some of the observed derivatization reactions with C_{60}^{2+} and, for molecules with sufficiently low ionization energies, can become the only reaction channel. However, electron transfer with C_{60}^{2+} occurs in the presence of an activation barrier that arises from coulomb repulsion between the charged product ions (see Fig. 14). Derivatization reactions also have been observed with C_{60}^{3+}, but electron transfer is even more competitive than with C_{60}^{2+}. For example, although ammonia has been reported to add to C_{60}^{3+}, only electron transfer has been seen with amines. Fig. 33 provides a summary of addition reactions observed with C_{60}^{3+}. New, charge separation, channels appear for some of the reactions with C_{60}^{3+}. For example, dissociative electron transfer to produce $C_{60}^{2+}/CH_2NH_2^+$ and C_{60}^{2+}/CH_3^+ is the dominant reaction channel with ethylamine. Also, dissociative addition

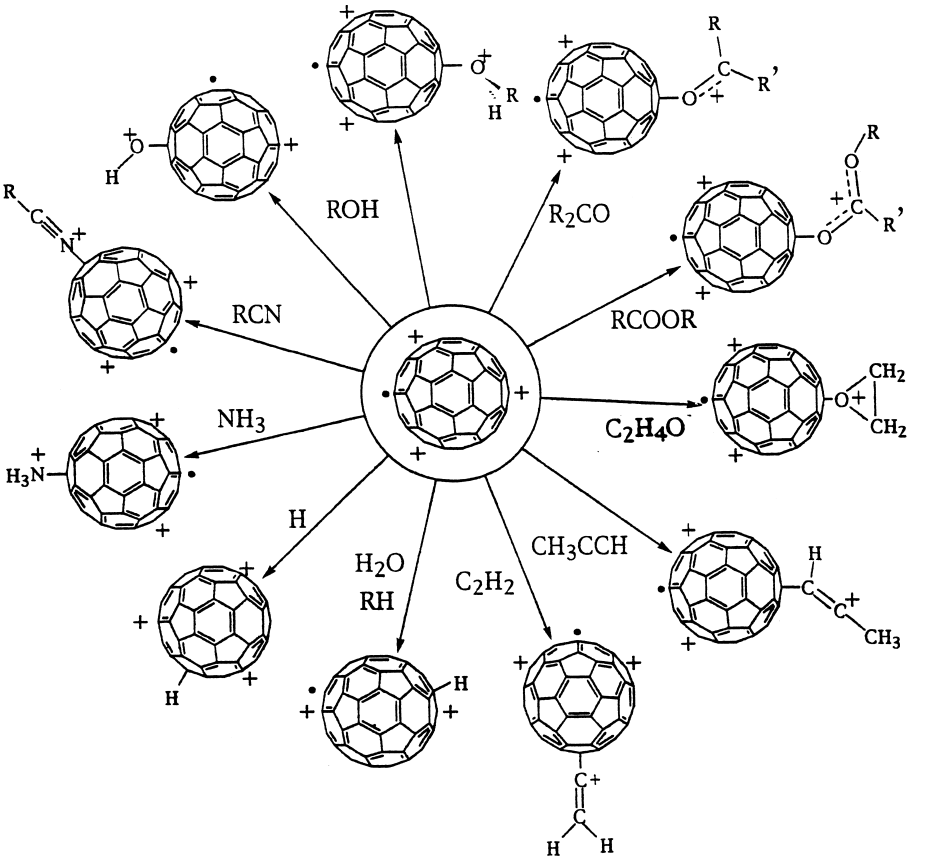

Fig. 33. An overview of derivatization reactions of C_{60}^{3+} observed with the York University SIFT apparatus at room temperature in helium buffer gas at 0.35 Torr [146]. The assigned structures are speculative.

reactions such as hydride and hydroxide transfer become more effective. This is the case with water, some alcohols and some alkanes. Halide transfer from HCl, HBr, and chlorinated methanes [153] also has been noted.

A generalized scheme for the observed higher-order chemistry initiated by fullerene cations is summarized in Fig. 34. Chemical derivatization of the fullerene surface has been surveyed for the first three charge states of C_{60} [146,154]. Both "fuzzy-ball" and "ball-and-chain" derivatization have been observed and multicollision induced dissociation experiments were used to differentiate between them. The former occurs with H atoms and nitriles in sequential addition reactions while methoxy derivatization was observed in sequential bimolecular methoxy-transfer reactions with methyl nitrite. A dramatic example of ball-and-chain derivatization is shown in Fig. 35 for the reaction of C_{60}^{2+} with allene [155]. The sequential addition of allene was characterized by an intriguing

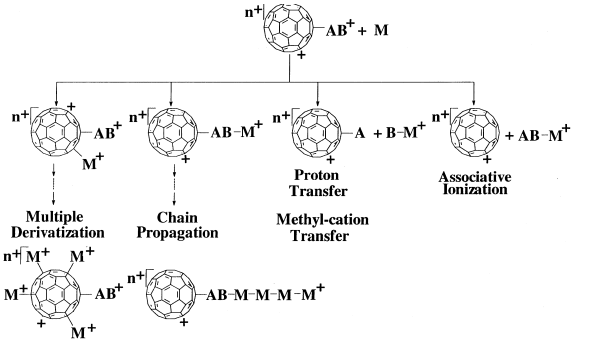

Fig. 34. Overview of the higher-order chemistry of C_{60} adduct ions with molecules M.

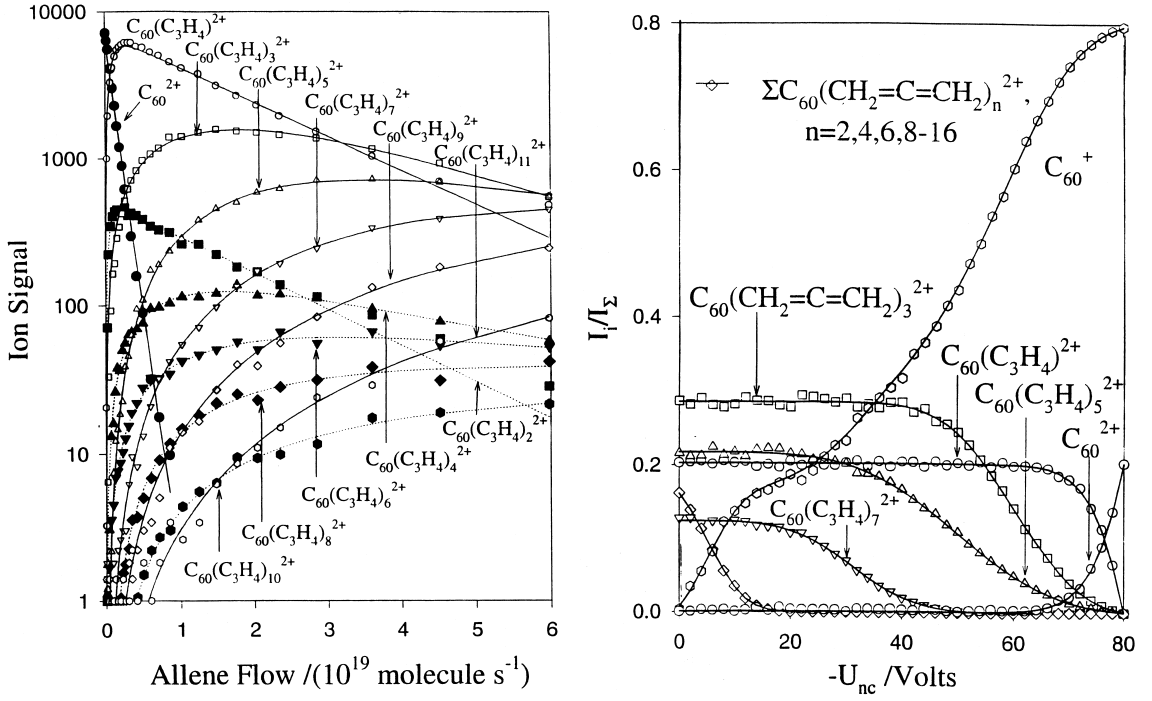

Fig. 35. (Left) Data for the sequential addition of allene to C_{60}^{2+} observed at a room temperature of 294 ± 2 K and a helium pressure of 0.35 ± 0.01 Torr. (Right) measured profiles for the multicollision-induced dissociation of $C_{60}(allene)^{2+}$ at an allene flow of 4.5×10^{19} molecules|s^{-1} in 10% argon/helium at a total pressure of 0.30 ± 0.01 Torr [149].

periodicity in rate with the even-numbered adducts reacting about 10 times faster than the odd adducts. These results have been interpreted in terms of the formation of the structure shown in Fig. 36. Apparently the ball-and-chain polymerization is driven by intramolecular coulombic repulsion between the somewhat delocalized charge on the C_{60} "anchor" and the more localized charge on the terminus of the growing chain. We first proposed this mechanism for polymerization of the well-known 1,3-butadiene monomer induced by C_{60}^{2+} [156]. Since then we have identified similar behaviour for the polymerization of ethylene oxide [157], 1-butene [158], allene and propyne [159], ethylene and acetylene [160], vinyl fluoride [161], and chlorinated ethylenes [152] initiated by C_{60}^{2+}, C_{70}^{2+} or C_{60}^{3+}. Not yet published are similar results of an investigation in our laboratory of reactions of the conventional diene monomers 1,3-butadiene, isoprene, cis- and trans-1,3 pentadiene, and 1,4-pentadiene, with the buckminsterfullerene cations $C_{60}^{\cdot+}$, C_{60}^{2+}, and C_{60}^{3+}. These latter experiments were directed toward a study of the influence of the nature and position of the substituent on the monomer and the effect of conjugation of the monomer on reactivity. Also, we have observed no end to the higher-order chemistry with methyl isocyanide as this

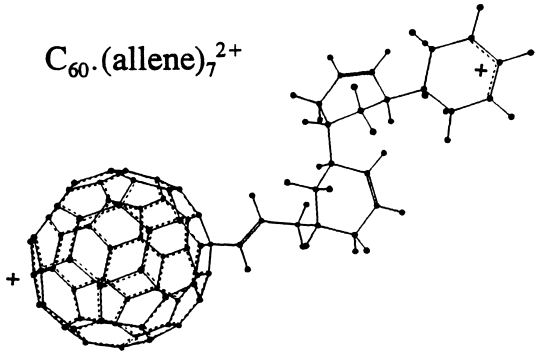

Fig. 36. Semi-empirical PM3 (parametric method) structure computed for $C_{60}(allene)_7^{2+}$ [149].

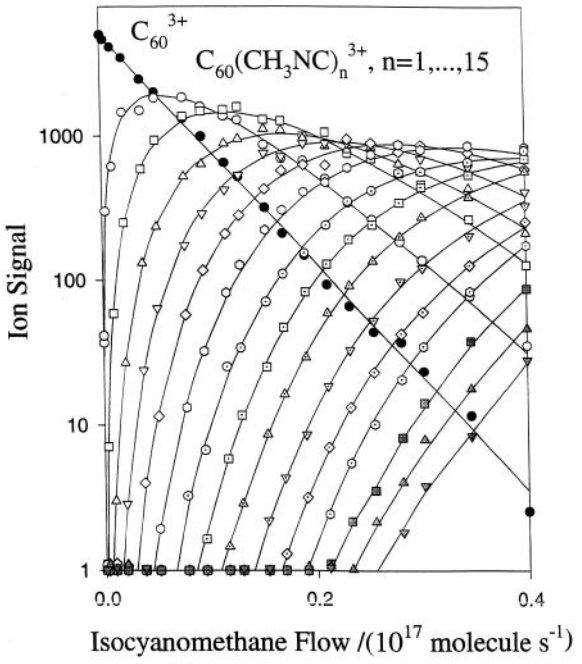

Fig. 37. Data for the sequential addition of methyl isocyanide to C_{60}^{3+} observed at a room temperature of 294 ± 2 K and a helium pressure of 0.35 ± 0.01 Torr.

monomer adds sequentially at least 15 times with no apparent decrease in rate (see Fig. 37). The chemistry initiated by C_{60}^{2+} in pyridine appears to lead to what is, so far, the only known example of the conversion of a ball-and-chain isomer to a "spindle" isomer [150].

We have observed that chain formation may be pre-empted if bimolecular formation of a dimer ion becomes exothermic for the reaction with the second monomer. This is the case for C_{60}^{3+} reacting with cyanides RCN with R = CN, C_2H_3, C_3H_3, and CH_2CN [162] as illustrated in

$$C_{60}(NCR)^{3+} + RCN \rightarrow C_{60}^{2+} + (RCN)_2^+ \qquad (24)$$

and for C_{60}^{2+} reacting with cyanoacetylene [162] as illustrated in

$$C_{60}(HC_3N)^{2+} + HC_3N \rightarrow C_{60}^{+} + (HC_3N)_2^+ \qquad (25)$$

These reactions appear to be driven by the stability of the product dimer cation. We have demonstrated with the aid of CID experiments and ab initio molecular orbital calculations [163] that dimerization in reaction (25) is accompanied by cyclization and that the structure and stability of $(HC_3N)_2^+$ is distinctly different from the structure of the dimer ion formed by the direct solvation of HC_3N^+ with HC_3N in the absence of C_{60}^{2+}. We have proposed that this isomer forms in a 2 + 2 cycloaddition of the second HC_3N molecule at the terminal carbon of the first HC_3N molecule attached through a nucleophilic attack of C_{60}^{2+} by its lone pair of electrons on the nitrogen atom [163]. The reaction profiles measured for the chemistry initiated by C_{60}^{2+} in HC_3N are shown in Fig. 38. The effective bimolecular rate coefficient, k, for the primary addition reaction is $7.3\ (\pm 2.4) \times 10^{-10}$ cm^3 molecule^{-1} s^{-1}. The secondary bimolecular reaction of $C_{60}(HC_3N)^{2+}$ with HC_3N results in charge separation, reaction (25), and occurs extremely rapidly, $k = 7.7\ (\pm 2.6) \times 10^{-9}$ cm^3 molecule^{-1} s^{-1}, essentially at the collision rate. Such a high rate is possible because of the large polarizability (5.29 Å^3) and dipole moment (μ_D = 3.72 Debye) of cyanoacetylene.

We also have investigated the influence of surface strain on the chemical reactivity of fullerene cations with a number of neutral reagents. Results for addition reactions of C_{56}^+, C_{58}^+, and C_{60}^+ with NH_3, of addition reactions of C_{56}^{2+}, C_{58}^{2+}, and C_{60}^{2+} with C_2H_4 and CH_3CN, and of hydride transfer reactions of C_{56}^{2+}, C_{58}^{2+}, and C_{60}^{2+} with n-C_4H_{10}, revealed a strong dependence of reactivity on the size of the fullerene cation [164]. The least-strained C_{60}^{n+} cations were found to be the least reactive as predicted [165]. Systematic studies of addition reactions of C_{56}^+, C_{58}^+, C_{60}^+, C_{70}^+, corannulene$^+$, and coronene$^+$ with cyclopentadiene and 1,3-cyclohexadiene indicated that the efficiency of bond formation depends strongly on the curvature of the carbonaceous surface as illustrated in Fig. 39 for addition reactions with cyclopentadiene [166].

12. Ionosheric, stratospheric, and planetary ion chemistry

As indicated earlier, the invention of flow-tube mass spectrometry was driven by the need to under-

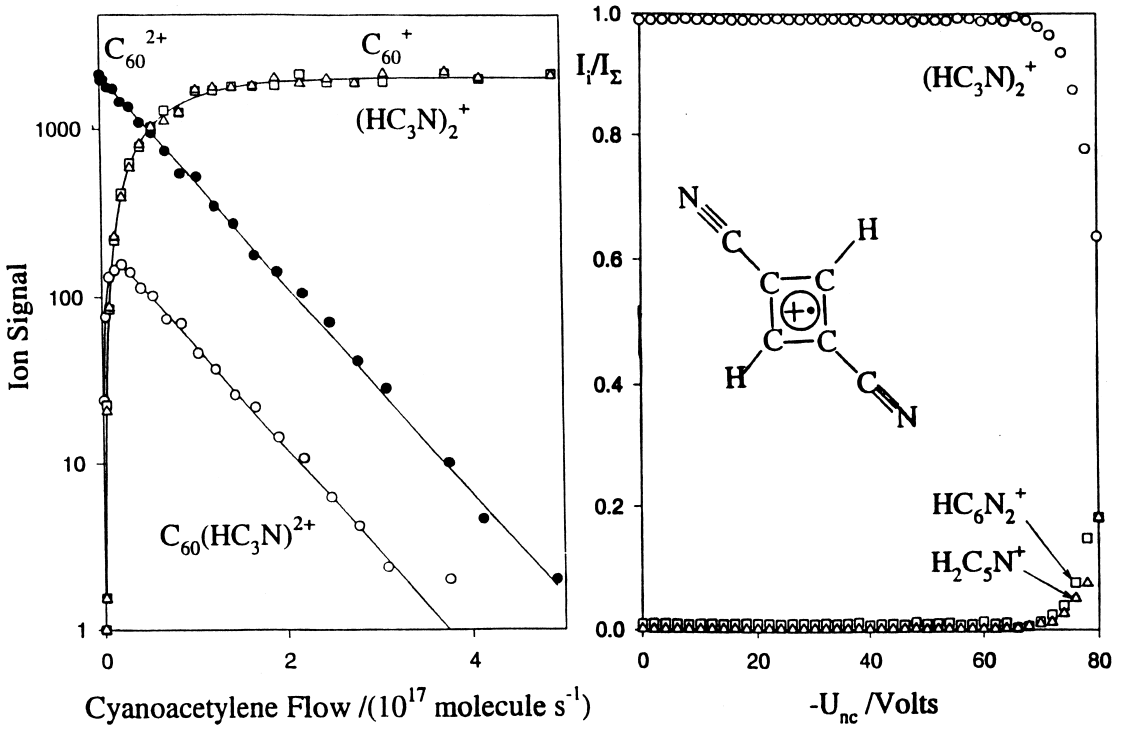

Fig. 38. (Left) Data for the sequential reactions of cyanoacetylene with C_{60}^{2+} observed at a room temperature of 294 ± 3 K and a helium pressure of 0.35 ± 0.01 Torr. (Right) measured profiles for the multicollision-induced dissociation of $(HC_3N)_2^+$ at a cyanoacetylene flow of 1.0×10^{17} molecules s^{-1} in 26% argon/helium. The rise in $HC_6N_2^+$ corresponds to the loss of H from the dimer cation and the rise of $H_2C_5N^+$ corresponds to loss of CN. The inserted structure corresponds to that calculated for the lowest-energy isomer on the potential-energy surface of $(HC_3N)_2^+$ which lies 64.7 kcal mol^{-1} below the energy of $HC_3N^+ + HC_3N$ [157].

stand the chemistry of the earth's ionosphere as part of a mission in radio propagation initiated by the US National Bureau of Standards in the early 1960s. At that time there were no rate coefficient data available for the many ion–molecule reactions that contribute to the ion chemistry occurring in the ionosphere. All this changed dramatically with the invention and directed use of the flow-tube mass spectrometer technique by Ferguson and his colleagues. Results of experimental measurements appeared, reaction by reaction, in several atmospheric journals until eventually, in less than about 10 years time, much of ionospheric chemistry was understood! And more than that, important fundamental aspects of the physical chemistry of ion–molecule reactions were identified and quantified for the first time. Several reviews by Eldon Ferguson provide detailed accounts of the individual ion–molecule reactions investigated in those early days [167], including metal–ion chemistry [168], and their impact on our understanding of the chemistry of the ionosphere [169,170].

Here, I should like to single out two accomplishments in particular: the measurements of ion–molecule reactions important in controlling electron densities in the F_2 region of the earth's ionosphere and the identification of the ion–molecule reactions that explained the origin of proton hydrates in the D region. The early FA measurements provided the first accurate rate coefficients for the reactions of O^+ with N_2 and O_2,

$$O^+ + N_2 \rightarrow NO^+ + N \quad (2)$$

$$O^+ + O_2 \rightarrow O_2^+ + O \quad (26)$$

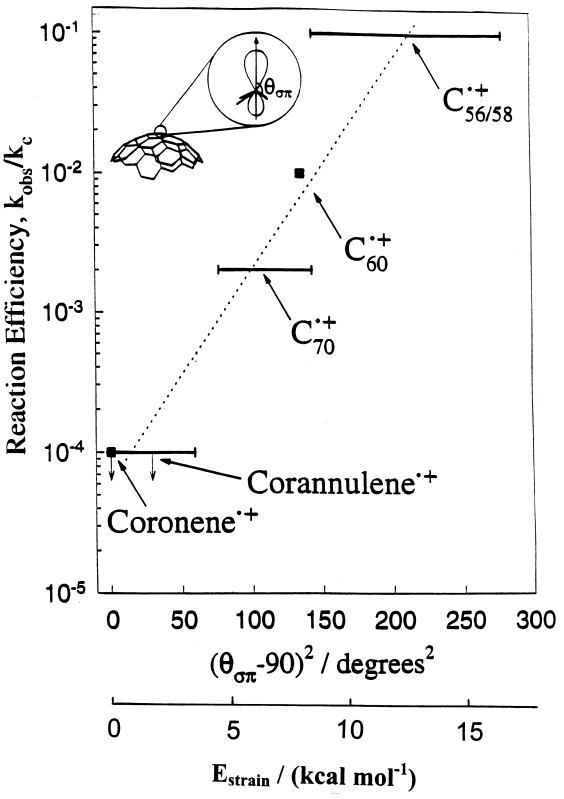

Fig. 39. A correlation between reaction efficiency, k_{obs}/k_c with the square of the POAV angle and the strain energy for addition reactions with cyclopentadiene at room temperature and a helium pressure of 0.35 ± 0.01 Torr [146]. k_{obs} is the measured rate coefficient and k_c is the collision rate coefficient which is estimated to be 10^{-9} cm^3 molecule^{-1} s^{-1}.

that convert atomic to molecular ions whose recombination rates with electrons are about 10^5 times greater than those for atomic ions. Dissociative recombination of the molecular ions produce electronically excited O atoms that radiate the nightglow, and electronically excited N(^{2}D) that reacts with O_2 to produce atmospheric NO. Reactions (2) and (26) are therefore important in the analysis of the airglow and atmospheric photochemistry, as well as to that of the electron density and ion composition of the ionosphere. The measurements showing that the O_2^+ and NO^+ water clusters convert to proton hydrates with increasing cluster size solved a long-standing problem in atmospheric chemistry that many other researchers could not. The following reaction illustrates the conversion that occurs with NO^+ water clusters:

$$NO^+(H_2O)_3 + H_2O \rightarrow H_3O^+(H_2O)_2 + HNO_2 \quad (27)$$

The complete positive ion–molecule reaction scheme proposed by Ferguson and his colleagues for D-region chemistry is shown in Fig. 40 [169,171]. Cosmic-ray ionization of N_2 and O_2 initiates ion chemistry in the stratosphere and troposphere and ultimately reactions of hydrated hydronium ions dominate this chemistry [169] (see Fig. 41).

Hydrated hydronium ions and their chemistry have been scrutinized in several laboratories using flow techniques. In 1989 Yang and Castleman observed "magic numbers" for $H_3O^+(H_2O)_n$ at 119 K for n = 21, 24, 26, and 28 and these ions were assigned clathrate-like structures [172]. Reactivity measurements with CH_3CN indicated a switch from proton transfer to simple association [172]. The temperature and cluster-size dependence of reactions of $H_3O^+(H_2O)_n$ with CH_3CN has received special attention by a number of groups [8,173,174] for more than 15 years (we had first looked at this reaction for n = 1 in 1976 [81]). Reactions of hydrated hydronium ions with n up to 30 have also been reported by the Castleman group with CH_3COCH_3 and CH_3COOCH_3 [175], N_2O_5 [176], and DNO_3 [177]. The results with N_2O_5 are of stratospheric chemistry interest since the following reaction is believed to occur heterogeneously on the surface of polar stratospheric cloud particles:

$$H_2O + N_2O_5 \rightarrow HNO_3 + HNO_3 \quad (28)$$

The flow-tube mass spectrometer experiments of Castleman and co-workers [176] provide evidence for the occurrence of reaction (28) within hydrated hydronium ions below 150 K according to the following reaction for $n \gtrsim 5$:

$$H_3O^+(H_2O)_n + N_2O_5 \rightarrow H_3O^+(H_2O)_{n-1}HNO_3 + HNO_3 \quad (29)$$

The reactions with DNO_3 also are interesting since it is argued that $D_3O^+(D_2O)_n$ reacts with DNO_3 by a

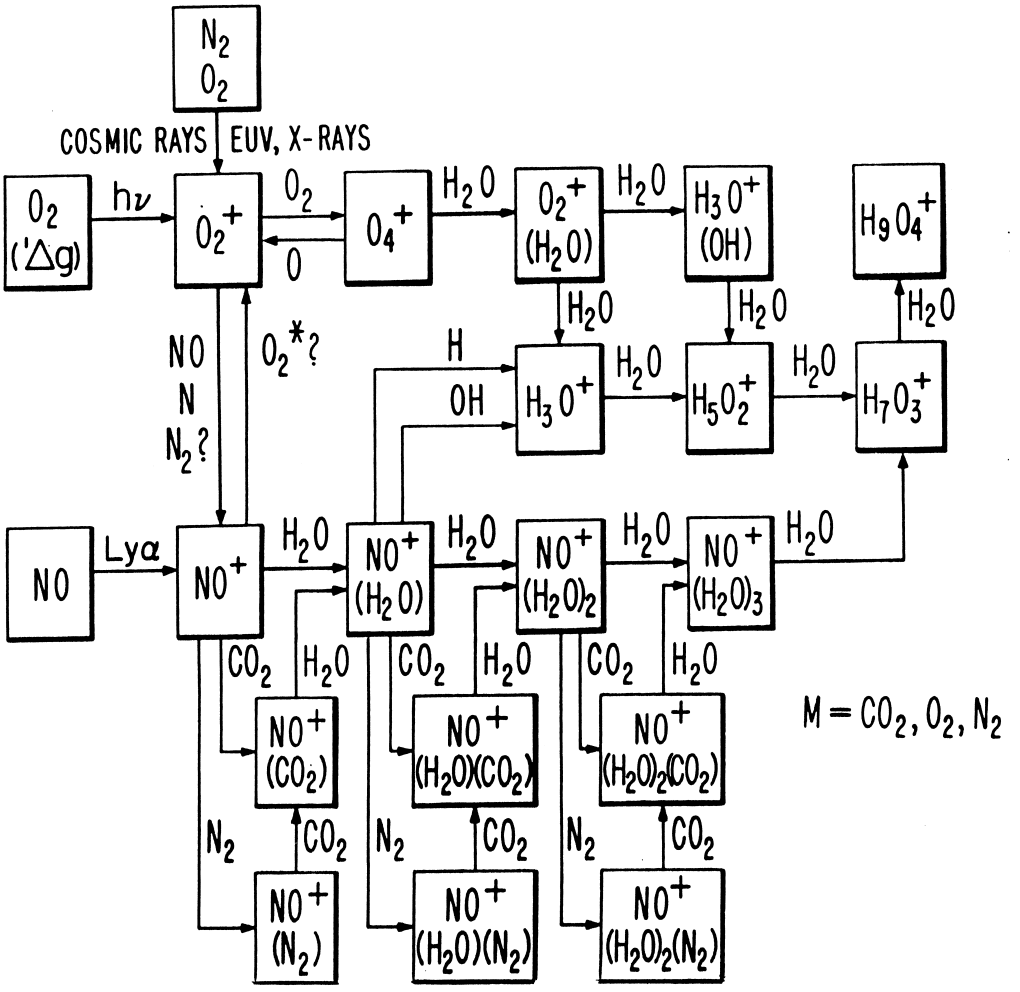

Fig. 40. Schematic diagram of the positive-ion chemistry proposed for the D region [169].

switching mechanism for $n \gtrsim 5$. As a consequence of further interest in the chemistry of the polar stratosphere, HCl uptake by (deuterated) hydrated hydronium ions has been investigated by the Castleman group with a flow-tube mass spectrometer over a range of pressure (0.26–0.46 Torr) and temperature (130–170 K) [178,179]

13. Interstellar/circumstellar ion chemistry

The proposal [180,181] that homogeneous ion–molecule reactions play a role in the formation of the large, complex molecules detected by radioastronomers in dense interstellar clouds, and the direct observation of ions such as CH^+, HCO^+, DCO^+, N_2H^+, and N_2D^+ in these environments, stimulated extensive measurements of reactions of these and related ions using flow-tube mass spectrometry. The Birmingham group was particularly active in this regard and a major focus of their SIFT measurements was the systematic study of reactions of hydrogenated ions, e.g. CH_n^+, $C_2H_n^+$, NH_n^+, H_nS^+, H_nCO^+, etc., with numerous molecular species [182]. Many of these reactions were investigated over the wide tem-

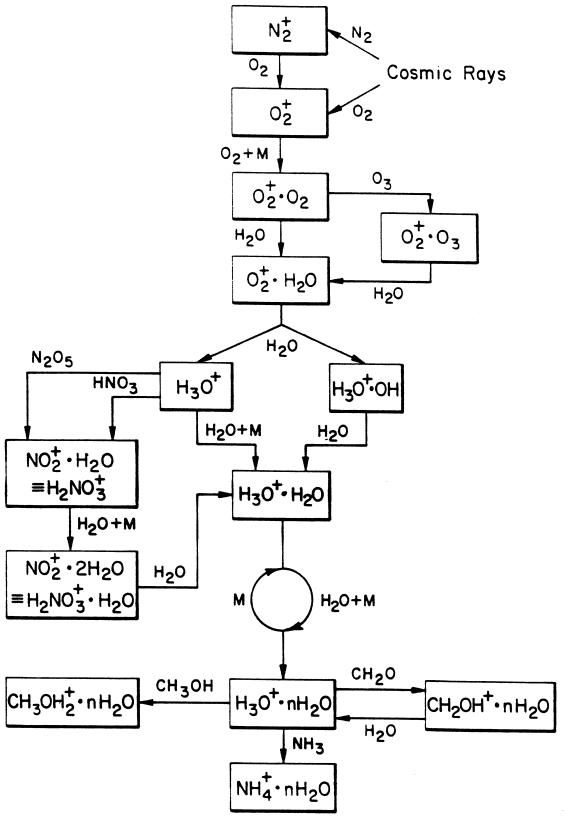

Fig. 41. Schematic diagram of the positive-ion chemistry proposed for the stratosphere and troposphere [169].

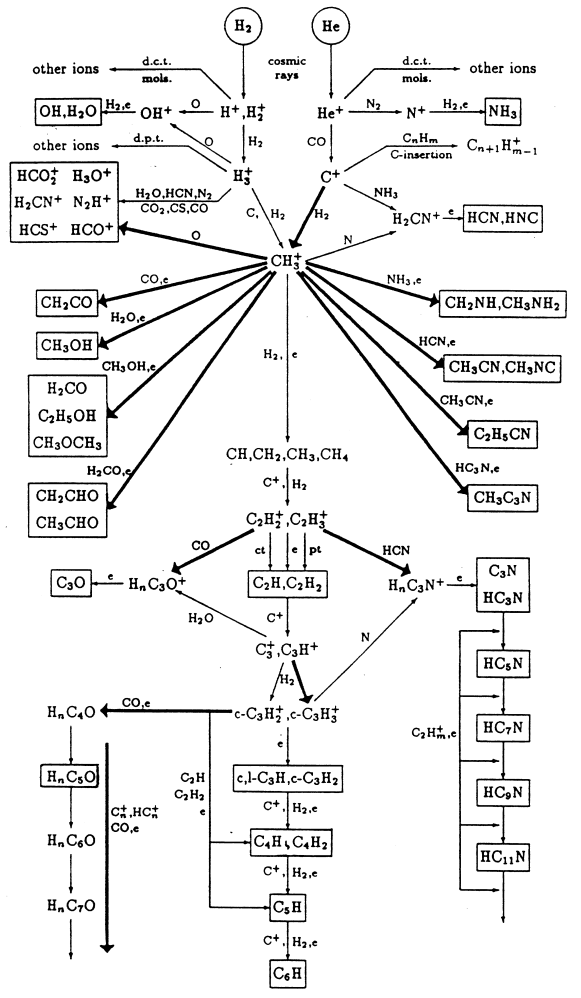

Fig. 42. Proposed positive-ion chemistry for dense interstellar clouds [182].

perature range from 80 to 600 K. The investigations have provided a large database (amounting to many hundreds of reaction rate coefficients and product ions) for the modeling of molecular synthesis in interstellar clouds. Fig. 42 presents an overview of the ion chemistry relevant to dense interstellar clouds that has been unraveled by the Birmingham group [182].

Observations that many interstellar ions (e.g. CH_3^+) rapidly associate with known interstellar molecules at low temperatures accentuated the importance of radiative association in the formation of interstellar molecules. Studies of ion association reactions that are potential sources for large interstellar molecules and of reactions between large hydrocarbon ions and atoms are continuing in the laboratory of Murray McEwan at the University of Canterbury [183,184].

Further contributions by the Birmingham group to interstellar physics and chemistry include detailed studies of isotope exchange in ion–neutral reactions, studies for which the SIFT is eminently suited, since the ion source gas and the reactant gas are not mixed. From these studies and detailed kinetic models of the interstellar ionic reactions, it is now understood that the observed enhancement of the rare isotopes (e.g. D, ^{13}C) in some interstellar molecules is due to the process of isotope fractionation in ion-neutral reactions [185]. Measurements of the rate coefficients for the reactions of the dipolar molecules HCl and HCN

at low temperatures provided the first experimental support for the theoretical prediction that the rate coefficients would increase rapidly with decreasing temperature, a most important result for interstellar chemistry.

The early emphasis on interstellar/circumstellar ion chemistry in our own laboratory was on the synthesis of hydrocarbon-chain and organonitrogen molecules [186,187], on ionic origins of carbenes [188] and on the formation of organosilicon molecules [189]. We have systematically explored the chemistry initiated by ground-state $Si^+(^2P)$, both free and attached to benzene and naphthalene, with a large variety of interstellar molecules [190,191]. It became clear from these studies that this chemistry provides plausible pathways to the synthesis of a variety of Si-bearing molecules including the SiC_4 chain molecule that was subsequently detected in circumstellar environments.

More recently we have begun to explore systematically the chemistry of organometallic and metal ions (Fe^+ and Mg^+) either free or attached to C_{60}, corannulene and several PAHs. Although there is as yet no convincing evidence for interstellar/circumstellar presence of C_{60}, we have proposed that C_{60} does serve as a useful model for carbonaceous dust [192]. On the basis of measured association rates of free Fe^+ ions with hydrocarbons, we have argued for the possible formation of the Fe-containing neutral molecules FeCO, FeC_2H_n and FeC_4H_n ($n = 1,2$) in dense interstellar clouds in the manner summarized in Fig. 43 [193]. Our measurements for the reaction of Mg^+ with ammonia have led to a proposal for the formation of circumstellar $MgNH_2$ [140]. As was the case with Si^+, we are finding that the reactivity of Fe^+ can be significantly altered when coordinated to a carbon network. Trapping on polycyclic aromatic hydrocarbons is thought to be a major loss process for atomic metal ions in the interstellar medium because of their inefficient recombination with electrons [192].

We have surveyed the implications of our experimental results for ion–molecule reactions involving fullerenes for interstellar and circumstellar chemistry [193] and have discussed the chemistry that possibly can lead to the chemical derivatization of fullerenes in

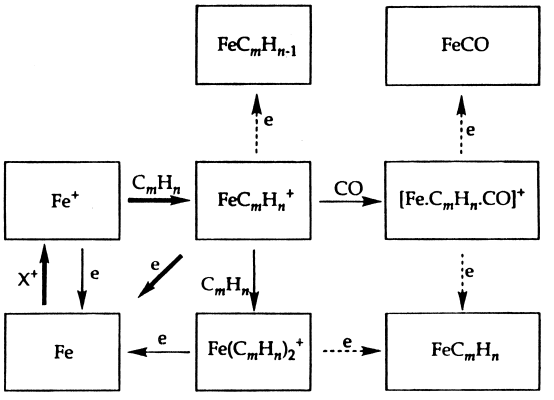

Fig. 43. Proposed reaction network for the formation of Fe-containing neutrals in dense interstellar clouds [192].

these environments [194]. On the basis of our observation of two-electron-transfer reactions of He^+ with naphthalene [67] and C_{60} [66], we have raised the possibility of the formation and production of large molecular di-cations by chemical ionization and their reaction by charge separation in the chemical evolution of cold interstellar clouds [195]. These charge separation reactions have the capacity to form internally cold but kinetically excited ions that can drive subsequent ion–molecule reactions that are endothermic at the ambient temperatures, e.g. H-atom transfer with H_2. Also, we have shown that intramolecular charge separation preceded by bonding to a doubly charged C_{60} (and so by inference doubly charged PAHs or C-containing grains) can lead to new synthetic pathways to cyclic cyanopolyenes [163].

14. Applications in analytical/medical chemistry

Arguably the first use of a flow-tube mass spectrometer as an analytical instrument for trace-gas analysis was reported in 1979 in a study of the products of the reaction of $O(^1D_2)$ with N_2O which were eluted from a radical reactor into the flow tube [196]. Six years later a modified FA technique, known as active chemical-ionization mass spectrometry (ACIMS), was reported for atmospheric trace-gas measurements in the free troposphere and lower stratosphere [197]. ACIMS relies on the chemical

ionization of trace-gas molecules in reactions with artificial, not ambient, ions (such as hydrated hydronium ions) that are formed in an ion source operated in ambient atmospheric air and carried by an air stream to a cryogenically pumped quadrupole mass spectrometer. The concentration of the reactant trace gas can be determined from the measured abundance ratio of reactant and product ions if the rate coefficients for the ion/molecule reactions connecting the two are known. Proton-transfer reactions involving hydrated hydronium ions were employed in the early application of ACIMS. The strength of the ACIMS method lies in its ability to provide real-time measurements at high spatial resolution as a consequence of its extreme sensitivity and very short response time [198]. Various atmospheric trace gases have been measured including acetonitrile, acetone and nitric acid by in situ aircraft-borne ACIMS measurements [197–199]. A SIFT mass spectrometer has recently been fitted with a supersonic cluster source by Viggiano and his colleagues to measure rate coefficients for reactions of hydrated hydronium ions of potential use in the chemical ionization detection of trace constituents in the atmosphere. They have found, for example, that CH_3SCH_3 reacts efficiently with hydrated hydronium ions with *n* up to 5, with the higher of these hydrates switching one H_2O for the CH_3SCH_3 [200]. Reactions with formaldehyde and acetaldehyde were investigated for their relevance to the chemistry of jet exhausts [201].

But the major breakthrough in the application of flow-tube mass spectrometry as a routine analytical instrument using positive-ion chemistry came about in the middle 1990s. An early version known as proton-transfer-reaction mass spectrometry (PTR-MS) developed by Hansel and Lindinger and their colleagues [202,203] made use of proton-transfer reactions proceeding in the flow-drift tube configuration. The SIFT configuration was employed by Spanel and Smith [204,205] in their SIFT-MS instrument that also makes use of electron-transfer, hydride transfer, hydroxide transfer and association reactions in addition to proton-transfer reactions for the chemical ionization of analytes. H_3O^+, O_2^+ and NO^+ have been found to be most suitable as chemical ionization reagents as they generally react with high efficiency with desired trace constituents and do not react rapidly with the common atmospheric bath gases N_2, O_2, H_2O, CO_2, and Ar. PTR-MS and SIFT-MS instruments, both of which have now been made portable, provide on-line real-time analysis of trace gas components with concentrations as low as a few pptv. The time response of these instruments is about 10^{-2} s and several components can be measured concomitantly by rapidly switching the downstream mass spectrometer between the chosen precursor and product ion masses. Spanel and Smith, using SIFT techniques, also are in the process of establishing a database in support of these analytical applications. Detailed studies are well under way of reactions of H_3O^+, NO^+, and O_2^+ with a series of organic compounds including alcohols, aldehydes, ketones, carboxylic acids, esters, ethers, amines, organosulphur compounds and hydrocarbons, and selected inorganic species of medical and environmental interest including NH_3, SO_2, NO, and NO_2 [90]. Breath analysis that allows the monitoring of metabolic processes in the human body has found medical application in clinical diagnosis and therapeutic monitoring. Measurements of volatile organic compound (VOC) emissions from fruit, coffee, and meat are of use in food research. VOC emissions from decaying biomatter have also been investigated as well as diurnal VOC variations in ambient air and these represent useful environmental applications.

Finally, last year, in our own laboratory, we began systematic measurements of reactions of isobaric ions with the aim of identifying reagent gases that may be employed to avoid isobaric interferences in the application of ICP/MS mass spectrometry to elemental analysis [15]. A commercial ICP torch (ELAN Series, Perkin Elmer-Sciex) has been attached to our SIFT for that purpose as described earlier. Recently we have reported reaction rate coefficients and product-ion distributions for the isobaric pairs ArO^+/Fe^+, Ar_2^+/Se^+, and ClO^+/V^+ reacting with a range of neutral modifiers [206]. Results obtained for the isobaric pair ArO^+/Fe^+ reacting with CO are shown in Fig. 44. The results of these measurements provide a database that permits the formulation of strategies for the use of

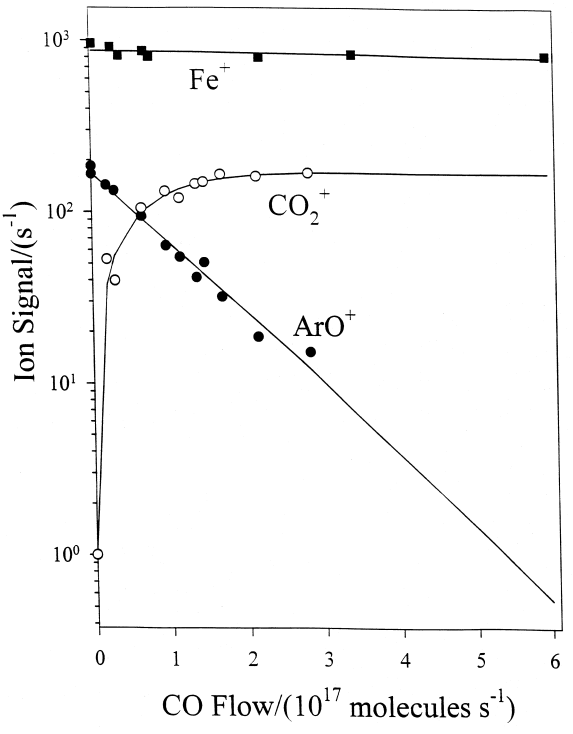

Fig. 44. ICP/SIFT results obtained for the isobaric pair ArO^+/Fe^+ reacting with CO [206].

ion–molecule reactions to move/remove isobaric interferences by adding reagent gases to an ICP/MS reaction cell (this procedure is known as chemical resolution) and so to improve quantitative detection limits.

Acknowledgements

The author has fond memories of his apprenticeship in Boulder/ESSA where he was introduced to the FA technique many years ago by Fred Fehsenfeld, Eldon Ferguson, and Art Schmeltekopf. Numerous co-workers have contributed to flow-tube mass spectrometry at York University over the years and the author is particularly grateful to all of them. Special thanks go to Nigel Adams, Albert Castleman, Chuck DePuy, Eldon Ferguson, Chava Lifshitz, Werner Lindinger, Murray McEwan, David Smith, and Al Viggiano for providing surveys of their own contributions to flow-tube mass spectrometry (which proved to be very useful in writing this review) and for their friendship over the years.

References

[1] D.K. Böhme, Ph.D., McGill University, 1965.
[2] R.S. Narcissi, A.D. Bailey, J. Geophys. Res. 70 (1965) 3687.
[3] E.E. Ferguson, J. Am. Soc. Mass Spectrom. 3 (1992) 479.
[4] E.E. Ferguson, F.C. Fehsenfeld, A.L. Schmeltekopf, Adv. At. Mol. Phys. 5 (1969) 1.
[5] S.T. Graul, R.R. Squires, Mass Spectrom. Rev. 7 (1988) 263.
[6] N.G. Adams, D. Smith, Int. J. Mass Spectrom. Ion. Phys. 21 (1976) 349.
[7] D. Smith, N.G. Adams, Adv. At. Mol. Phys. 24 (1988) 1.
[8] A.A. Viggiano, F. Dale, J.F. Paulson, J. Chem. Phys. 88 (1988) 2469.
[9] D.W, Fahey, H. Bhringer, F.C. Fehsenfeld, E.E. Ferguson, J. Chem. Phys. 76 (1982) 1799.
[10] X. Yang, Z. Zhang, A.W. Castleman, Int. J. Mass Spectrom. Ion Processes 109 (1991) 339.
[11] A.A. Viggiano, S.T. Arnold, R.A. Morris, Int. Rev. Phys. Chem. 17 (1998) 147.
[12] J.D. Poutsma, R.A. Seburg, L.J. Cgyall, L.S. Sunderlin, B.T. Hill, J. Hu, R.R. Squires, Rapid. Commun. Mass Spectrom. 11 (1997) 489.
[13] G. Koster, M. Soskin, M. Peres, C. Lifshitz, Int. J. Mass Spectrom. 179/180 (1998) 165.
[14] G. Koster, C. Lifshitz, Int. J. Mass Spectrom. 182/183 (1999) 213.
[15] G.K. Koyanagi, V.V. Lavrov, V. Baranov, D. Bandura, S. Tanner, J.W. McLaren, D.K. Böhme, Int. J. Mass Spectrom. 194 (2000) L1.
[16] A.L. Schmeltekopf, E.E. Ferguson, F.C. Fehsenfeld, J. Chem Phys. 48 (1968) 2966.
[17] E.E. Ferguson, F.C. Fehsenfeld, P.D. Goldan, A.L. Schmeltekopf, H.I. Schiff, Planet. Space Sci. 13 (1965) 823.
[18] See, for example G.B.I. Scott, D.A. Fairley, C.G. Freeman, M.J. McEwan, V.G. Anicich, J. Phys. Chem. A 103 (1999) 1073.
[19] D.B. Dunkin, F.C. Fehsenfeld, A.L. Schmeltekopf, E.E. Ferguson, J. Chem. Phys. 49 (1968) 1365.
[20] W. Lindinger, F.C. Fehsenfeld, A.L. Schmeltekopf, E.E. Ferguson, J. Geophys. Res. 79 (1974) 4753.
[21] P.M. Hierl, J.F. Friedman, T.M. Miller, I. Dotan, M. Menendesz-Baretto, J.V. Seeley, T.S. Williamson, F. Dale, P.L. Mundis, R.A. Morris, J.F. Paulson, A.A. Viggiano, Rev. Sci. Instrum. 67 (1996) 2142.
[22] P.M. Hierl, I. Dotan, J.V. Seeley, J.M. Van Doren, R.A. Morris, A.A. Viggiano, J. Chem. Phys. 106 (1997) 3540.
[23] A.A. Viggiano, R.A. Morris, F. Dale, J.F. Paulson, K. Giles, D. Smith, T. Su, J. Chem. Phys. 93 (1990) 1149.
[24] M. McFarland, D.L. Albritton,, F.C. Fehsenfeld, E.E. Ferguson, A.L. Schmeltekopf, J. Chem. Phys. 59 (1973) 6610.

[25] See, for example W. Lindinger, Int. J. Mass Spectrom. Ion Processes 80 (1987) 115.
[26] N.G. Adams, D. Smith, Int. J. Mass Spectrom. Ion Phys. 21 (1976) 349.
[27] D. Smith, N.G. Adams, in Gas-Phase Ion Chemistry, M.T. Bowers (Ed.), Academic, New York, !979, Vol. 1, pp. 1–44.
[28] D. Smith, N.G. Adams, E. Alge, Chem. Phys. Lett. 105 (1984) 317.
[29] D. Smith, N.G. Adams Swarms of Ions and Electrons in Gases, W. Lindinger, T.D. Märk, F. Howorka (Eds.), Springer, Vienna, 1984, pp. 284–306.
[30] O. Chudácek, P. Kudrna, J. Glosík, M. Äicha, M. Tichý, Contrib. Plasma Phys. 35 (1995) 503.
[31] L.D. Schearer, Phys. Rev. A 10 (1974) 1380.
[32] R.R. Squires, Int. J. Mass Spectrom. Ion Processes 118/119 (1992) 503.
[33] P.J. Marinelli, J.A. Paulino, L.S. Sunderlin, P.G. Wenthold, J.C. Poutsma, R.R. Squires, Int. J. Mass Spetrom. Ion Processes 130 (1994) 89.
[34] V. Baranov, D.K. Böhme, Int. J. Mass Spectrom. Ion Processes 154 (1996) 71.
[35] E.E. Ferguson, J. Mass Spec. Ion Processes 80 (1987) 81.
[36] N.G. Adams, D. Smith, J. Phys. B 9 (1976) 1439.
[37] See, for example D.K. Böhme, R.S. Hemsworth, H.W. Rundle, H.I. Schiff, J. Chem. Phys. 58 (1973) 3504.
[38] See, for example R.S. Hemsworth, H.W. Rundle, D.K. Böhme, H.I. Schiff, D.B. Dunkin, F.C. Fehsenfeld, J. Chem. Phys. 59 (1973) 61.
[39] W. Lindinger, F.C. Fehsenfeld, A.L. Schmeltekopf, E.E. Ferguson, J. Geophys. Res. 79 (1974) 4753.
[40] P.M. Hierl, I. Dotan, J.V. Seeley, J.M. Van Doren, R.A. Morris, A.A. Viggiano, J. Chem. Phys. 106 (1997) 3540.
[41] S.T. Arnold, A.A. Viggiano, R.A. Morris, J. Phys. Chem. A 101 (1997) 9351.
[42] S.T. Arnold, A.A. Viggiano, R.A. Morris, J. Phys. Chem. A 102 (1998) 8881.
[43] S.T. Arnold, S. Williams, I. Dotan, A.J. Midey, A.A. Viggiano, R.A. Morris, J. Phys. Chem. A 103 (1999) 8421.
[44] S.T. Arnold, I. Dotan, S. Williams, A.A. Viggiano, R.A. Morris, J. Phys. Chem. A 104 (2000) 928.
[45] A.J. Midey, S. Williams, S.T. Arnold, I. Dotan, R.A. Morris, A.A. Viggiano, Int. J. Mass Spectrom. 195 (2000) 327.
[46] A.A. Viggiano, R.A. Morris, J. Phys. Chem. 100 (1996) 19227.
[47] W. Lindinger, M. McFarland, F.C. Fehsenfeld, D.L. Albritton, A.L. Schmeltekopf, E.E. Ferguson, J. Chem. Phys. 63 (1975) 2175.
[48] E.E. Ferguson, J. Phys. Chem. 90 (1986) 731.
[49] S. Kato, M.J. Frost, V.M. Bierbaum, S.R. Leone, Rev. Sci. Instrum. 64 (1993) 2808.
[50] N.G. Adams, D. Smith, E.E. Ferguson, Int. J. Mass Spectrom. Ion Processes 67 (1985) 67.
[51] S.E. Barlow, J.M. Van Doren, C.H. DePuy, V.M. Bierbaum, I. Dotan, E.E. Ferguson, N.G. Adams, D. Smith, B.R. Rowe, J.D. Marquette, G. Dupeyrat, M. Durup-Ferguson, J. Chem. Phys. 85 (1986) 3851.
[52] A.A. Viggiano, R.A. Morris, F. Dale, J.F. Paulson, K. Giles, D. Smith, T. Su, J. Chem. Phys. 93 (1990) 1149.
[53] F.C. Fehsenfeld, E.E. Ferguson, J. Chem. Phys. 56 (1972) 3066.
[54] A.L. Schmeltekopf, F.C. Fehsenfeld, E.E. Ferguson, J. Chem. Phys. 48 (1968) 2966.
[55] M. Tsuji, H. Kouno, K. Matsumura, T. Funatsu, Y. Nikishima, H. Obase, H. Kugishima, K. Yoshida, J. Chem. Phys. 98 (1993) 2011.
[56] C. Praxmarer, A. Hansel, W. Lindinger, Z. Herman, J. Chem. Phys. 109 (1998) 4246.
[57] T.D. Williams, L.M. Babcock, N.G. Adams, Int. J. Mass Spectrom. 185/186/187 (1999) 759.
[58] E.E. Ferguson, J.M. Van Doren, A.A. Viggiano, R.A. Morris, J.F. Paulson, J.D. Stewart, L.S. Sunderlin, P.B. Armentrout, Int. J. Mass Spectrom. Ion Processes 117 (1992) 261.
[59] K. Giles, N.G. Adams, D. Smith, J. Phys. B 22 (1989) 873.
[60] K.G. Spears, F.C. Fehsenfeld, M. McFarland, E.E. Ferguson, J. Chem. Phys. 56 (1972) 2562.
[61] D. Smith, N.G. Adams, E. Alge, H. Villinger, W. Lindinger, J. Phys. B 13 (1980) 2787.
[62] D. Smith, D. Grief, N.G. Adams, Int. J. Mass Spectrom. Ion Phys. 30 (1979) 271.
[63] N.G. Adams, D. Smith, D. Grief, J. Phys. B 12 (1979) 791.
[64] N.G. Adams, D. Smith, Int. J. Mass Spectrom. Ion Phys. 35 (1980) 335.
[65] D.K. Böhme, Int. Rev. Phys. Chem. 13 (1994) 163.
[66] G. Javahery, S. Petrie, J. Wang, D.K. Böhme, Chem. Phys. Lett. 195 (1992) 7.
[67] S. Petrie, G. Javahery, A. Fox, D.K. Böhme, J. Phys. Chem. 97 (1993) 5607.
[68] S. Petrie, J. Javahery, J. Wang, D.K. Böhme, J. Phys. Chem. 96 (1992) 6121.
[69] G. Javahery, H. Wincel, S. Petrie, D.K. Böhme, Chem. Phys. Lett. 204 (1993) 467.
[70] G. Javahery, H. Becker, S. Petrie, P.C. Cheng, H. Schwarz, L.T. Scott, D.K. Böhme, Org. Mass Spectrom. 20 (1993) 1005.
[71] J.A. Burt, J.L. Dunn, M.J. McEwan, M.M. Sutton, A.E. Roche, H.I. Schiff, J. Chem. Phys. 52 (1970) 6062.
[72] A.E. Roche, M.M. Sutton, D.K. Böhme, H.I. Schiff, J. Chem. Phys. 55 (1971) 5480.
[73] D.K. Böhme, R.S. Hemsworth, H.W. Rundle, H.I. Schiff, J. Chem. Phys. 58 (1973) 3504.
[74] R.S. Hemsworth, H.W. Rundle, D.K. Böhme, H.I. Schiff, D.B. Dunkin, F.C. Fehsenfeld, J. Chem. Phys. 59 (1973) 61.
[75] D.K. Böhme, G.I. Mackay, H.I. Schiff, J. Chem. Phys. 73 (1980) 4976.
[76] K. Tanaka, G.I. Mackay, D.K. Böhme, Can. J. Chem. 56 (1978) 193.
[77] D.K. Böhme, G.I. Mackay, J. Am. Chem. Soc. 103 (1981) 2173.
[78] D.K. Böhme, in Interactions Between Ions and Molecules, P. Ausloos (Ed.), Plenum, New York, 1975, pp. 489–504.
[79] R.S. Hemsworth, J.D. Payzant, H.I. Schiff, D.K. Böhme. Chem. Phys. Lett. 26 (1974) 417.
[80] D. Betowski, J.D. Payzant, G.I. Mackay, D.K. Böhme, Chem. Phys. Lett. 31 (1975) 321.
[81] G.I. Mackay, L.D. Betowski, J.D. Payzant, H.I. Schiff, D.K. Böhme, J. Phys. Chem. 80 (1976) 2919.

[82] G.I. Mackay, D.K. Böhme, Int. J. Mass Spectrom. Ion Phys. 26 (1976) 327.
[83] S.D. Tanner, G.I. Mackay, D.K. Böhme, Can. J. Chem. 57 (1979) 2350.
[84] G.I. Mackay, K. Tanaka, D.K. Böhme, Int. J. Mass Spectrom. Ion Phys. 24 (1975) 125.
[85] S.D. Tanner, G.I. Mackay, A.C. Hopkinson, D.K. Böhme, Int. J. Mass Spectrom. Ion Phys. 29 (1979) 153.
[86] G.I. Mackay, S.D. Tanner, A.C. Hopkinson, D.K. Böhme, Can. J. Chem. 57 (1979) 1518.
[87] G.I. Mackay, A.C. Hopkinson, D.K. Böhme, J. Am. Chem. Soc. 100 (1978) 7460.
[88] A.C. Hopkinson, G.I. Mackay, D.K. Böhme, Can. J. Chem. 57 (1979) 2996.
[89] G.I. Mackay, H.I. Schiff, D.K. Böhme, Can. J. Chem. 59 (1981) 1771.
[90] See, for example P. Spanel, D. Smith, Int. J. Mass Spectrom. 181 (1998) 1.
[91] M. Henchman, D. Smith, N.G. Adams, Int. J. Mass Spectrom. Ion Processes 109 (1991) 105.
[92] D.K. Böhme, Int. J. Mass Spectrom. Ion Processes 115 (1992) 95.
[93] A.J. Chalk, L. Radom, J. Am. Chem. Soc. 119 (1997) 7573.
[94] A. Cunje, C.F. Rodriquez, D.K. Böhme, A.C. Hopkinson, J. Phys. Chem. 102 (1998) 478.
[95] A. Cunje, C.F. Rodriquez, D.K. Böhme, A.C. Hopkinson, Can. J. Chem. 76 (1998) 1138.
[96] See, for example M.A. Trikoupis, J.K. Terlow, P.C. Burgers, J. Am. Chem. Soc. 120 (1998) 12131.
[97] V. Baranov, S. Petrie, D.K. Böhme, J. Am. Chem. Soc. 118 (1996) 4500.
[98] D.K. Böhme, G.I. Mackay, S.D. Tanner. J. Am. Chem. Soc. 101 (1979) 3724.
[99] D.K. Böhme, in Ionic Processes in the Gas Phase, M.A. Almoster Ferreira (Ed.), Reidel, New York, 1984, pp.111–134.
[100] D.K. Böhme Transactions of the Royal Society of Canada, Fourth Series, XIX (1981) 265.
[101] D. Smith, N.G. Adams, M.J. Henchman, J. Chem. Phys. 72 (1980) 4951.
[102] S. Petrie, G. Javahery, D.K. Böhme, Int. J. Mass Spectrom. Ion Processes 124 (1993) 145.
[103] S. Petrie, D.K. Böhme, J. Am. Soc. Mass Spectrom. 9 (1998) 114.
[104] S. Petrie, G. Javahery, H. Wincel, J. Wang, D.K. Böhme, J. Am. Chem. Soc. 115 (1993) 6290.
[105] V. Baranov, D.K. Böhme, Chem. Phys. Lett. 258 (1996) 203.
[106] D. Smith, N.G. Adams, in Physics of Ion–ion and Electron–ion Collisions, F. Brouillard, J.W. McGowan (Eds.), Plenum, Nw York, 1983, pp. 501–531.
[107] N.G. Adams, D. Smith, in Dissociative Recombination: Theory, Experiment and Applications, J.B.A. Mitchell, S.L. Guberman (Eds.), World Scientific, Singapore, 1988, pp. 124–140.
[108] M Larsson, Annu. Rev. Phys. Chem. 48 (1997) 151.
[109] N.G. Adams, C.R. Herd, D. Smith, J. Chem. Phys. 91 (1989) 963.
[110] C.R. Herd, N.G. Adams, D. Smith, Ap. J. 349 (1990) 388.
[111] N.G. Adams, C.R. Herd, M. Geoghegan, D. Smith, A. Canosa, J.C. Gomet, B.R. Rowe, J.L. Queffelec, M. Morlais, J. Chem. Phys. 94 (1991) 4852.
[112] J.M. Butler, L.M. Babcock, N.G. Adams, Mol. Phys. 91 (1997) 81.
[113] B.L. Foley, N.G. Adams, H.S. Lee, J. Phys. Chem. 97 (1993) 5218.
[114] N.G. Adams, L.M. Babcock, J. Phys. Chem. 98 (1994) 4564.
[115] N.G. Adams, Int. J. Mass Spectrom. Ion Processes 132 (1994) 1.
[116] K.G. Spears, E.E. Ferguson, J. Chem. Phys. 59 (1973) 4174.
[117] E.E. Ferguson, B.R. Rowe, D.W. Fahey, F.C. Fehsenfeld, Planet. Space Sci. 29 (1981) 479.
[118] K.G. Spears, F.C. Fehsenfeld, J. Chem. Phys. 56 (1972) 5698.
[119] F.C. Fehsenfeld, Can. J. Chem. 47 (1969) 1808.
[120] E.E. Ferguson, D.W. Fahey, F.C. Fehsenfeld, D.L. Albritton, Planet. Space Sci 29 (1981) 307.
[121] K.G. Spears, F.C. Fehsenfeld, M. McFarland, E.E. Ferguson, J. Chem. Phys. 56 (1972) 2562.
[122] B.R. Rowe, A.A. Viggiano, F.C. Fehsenfeld, D.W. Fahey, E.E. Ferguson, J. Chem. Phys. 76 (1982) 742.
[123] A.A. Viggiano, C.A. Deakyne, F. Dale, J.H. Paulson, J. Chem. Phys. 87 (1987) 6544.
[124] L. Capron, W.Y. Feng, C. Lifshitz, B.L. Tjelta, P.B. Armentrout, J. Phys. Chem. 100 (1996) 16571.
[125] A.W. Castleman, K.G. Weil, S.W. Sigsworth, R.E. Leuchtner, R.G. Keesee, J. Chem. Phys. 86 (1987) 3829.
[126] R. Passarella, A.W. Castleman, J. Phys. Chem. 93 (1989) 5840.
[127] X. Yang, A.W. Castleman, J. Chem. Phys. 93 (1990) 2405.
[128] S.W. Sigsworth, A.W. Castleman, Chem. Phys. Lett. 168 (1990) 314.
[129] A.G. Harms, S.N. Khanna, B. Chen, A.W. Castleman, J. Chem. Phys. 100 (1994) 3540.
[130] X. Zhang, A.W. Castleman, J. Am. Chem. Soc. 114 (1992) 8607.
[131] A. Selinger, A.W. Castleman, J. Phys. Chem. 95 (1991) 8442.
[132] R. Tonkyn, M. Ronan, J.C. Weisshaar, J. Phys. Chem. 92 (1988) 92.
[133] W.S. Taylor, W.R. Everett, L.M. Babcock, T.L. McNeil, Int. J. Mass Spectrom. Ion Processes 125 (1993) 45.
[134] V.I. Baranov, G. Javahery, A.C. Hopkinson, D.K. Böhme, J. Am. Chem. Soc. 117 (1995) 12801.
[135] V.I. Baranov, G. Javahery, D.K. Böhme, Chem. Phys. Lett. 239 (1995) 339.
[136] D. Schröder, H. Schwarz, D.E. Clemmer, Y. Chen, P.B. Armentrout, V.I. Baranov, D.K. Böhme, Int. J. Mass Spectrom. Ion Processes 161 (1997) 175.
[137] V. Baranov, H. Becker, D.K. Böhme, J. Phys. Chem. A 101 (1997) 5137.

[138] R.K. Milburn, V. Baranov, A.C. Hopkinson, D.K. Böhme, J. Phys. Chem. 102 (1998) 9803.
[139] V. Baranov, D.K. Böhme, Int. J. Mass Spectrom., in press.
[140] R.K. Milburn, V. Baranov, A.C. Hopkinson, D.K. Böhme, J. Phys. Chem. 103 (1999) 6373.
[141] R.K. Milburn, M.V. Frash, A.C. Hopkinson, D.K. Böhme, J. Phys. Chem. A 104 (2000) 3926.
[142] D.K. Böhme, S. Wlodek, H. Wincel, J. Am. Chem. Soc. 113 (1991) 6396.
[143] D.K. Böhme, Chem. Rev. 92 (1992) 1487.
[144] V.I. Baranov, D.K. Böhme. Int. J. Mass Spectrom. Ion Processes 149/150 (1995) 543.
[145] R.E. Leuchtner, A.C. Harms, A.W. Castleman, J. Chem. Phys. 92 (1990) 6527.
[146] D.K. Böhme, Can. J. Chem. 77 (1999) 1453.
[147] S. Petrie, D.K. Böhme, Can. J. Chem. 72 (1994) 577.
[148] D.K. Böhme, in Recent Advances in the Chemistry and Physics of Fullerenes and Related Materials, R.S. Ruoff, K.M. Kadish (Eds.), Electrochemical Society Proceedings Vol. 97-14, Electrochemical Society, Pennington, NJ, 1997, p. 763.
[149] J. Sun, D.K. Böhme, Int. J. Mass Spectrom. 195/196 (2000) 401.
[150] J. Sun, D.K. Böhme, Int. J. Mass Spectrom. 179/180 (1998) 267.
[151] V. Baranov, D.K. Böhme, Int. J. Mass Spectrom. Ion Processes 165/166 (1997) 249.
[152] Y. Ling, G.K. Koyanagi, D. Caraiman, A.C. Hopkinson, D.K. Böhme, Int. J. Mass Spectrom. 192 (1999) 215.
[153] Y. Ling, G.K. Koyanagi, D. Caraiman, V. Baranov, D.K. Böhme, Int. J. Mass Spectrom. 182/183 (1999) 349.
[154] D.K. Böhme, in Recent Advances in the Chemistry and Physics of Fullerenes and Related Materials, R.S. Ruoff, K.M. Kadish (Eds.), Electrochemical Society Proceedings 95-10, Electrochemical Society, Pennington, NJ, 1995, p. 1465.
[155] V. Baranov, J.Wang, A.C. Hopkinson, D.K. Böhme, J. Am. Chem. Soc. 119 (1997) 2040.
[156] J. Wang, G. Javahery, S. Petrie, D.K. Böhme, J. Am. Chem. Soc. 114 (1992) 9665.
[157] J. Wang, G. Javahery, S. Petrie, A.C. Hopkinson, D.K. Böhme, Angew. Chem. Int. Ed. Engl. 33 (1994) 206.
[158] J. Wang, V. Baranov, D.K. Böhme, J. Am. Soc. Mass Spectrom. 7 (1990) 261.
[159] V. Baranov, J.Wang, A.C. Hopkinson, D.K. Böhme, J. Am. Chem. Soc. 119 (1997) 2040.
[160] J. Wang, G. Javahery, V. Baranov, D.K. Böhme, Tetrahedron 52 (1996) 5191.
[161] Y. Ling, D.K. Böhme, Eur. Mass Spectrom. 5 (1999) 471.
[162] G. Javahery, S. Petrie, J. Wang, H. Wincel, D.K. Böhme, J. Am. Chem. Soc. 115 (1993) 9701.
[163] R.K. Milburn, A.C. Hopkinson, J. Sun, D.K. Böhme, J. Phys. Chem. 103 (1999) 7528.
[164] S. Petrie, D.K. Böhme, Nature 165 (1993) 426.
[165] R.C. Haddon, Science 261 (1993) 1545.
[166] H. Becker, L.T. Scott, D.K. Böhme, Int. J. Mass Spectrom. Ion Processes 167/168 (1997) 519.
[167] E.E. Ferguson, Rev. Geophys. Space Phys. 12 (1974) 703.
[168] E.E. Ferguson, Radio Sci. 7 (1972) 397.
[169] E.E. Ferguson, in Interactions Between Ions and Molecules, P. Ausloos (Ed.), Plenum, New York 1975, pp. 377–403.
[170] E.E. Ferguson, J. Mass Spectrom. 32 (1273 (1997).
[171] E.E. Ferguson, F.C. Fehsenfeld, J. Geophys. Res. Space Phys. 74 (1969) 5743.
[172] X. Yang, A.W. Castleman, J. Am. Chem. Soc. 111 (1989) 6845.
[173] D. Smith, N.G. Adams, E. Alge, Planet. Space Sci. 29 (1981) 449.
[174] X. Yang, A.W. Castleman, J. Chem. Phys. 95 (1991) 130.
[175] X. Yang, X. Zhang, A.W. Castleman, Int. J. Mass Spectrom. Ion Processes 109 (1991) 339.
[176] H. Wincel, E. Mereand, A.W. Castleman, J. Phys. Chem. 98 (1994) 8606.
[177] X. Zhang, E.L. Mereand, A.W. Castleman, J. Phys. Chem. 98 (1994) 3554.
[178] R.S. MacTaylor, J.J. Gilligan, D.J. Moody, A.W. Castleman, J. Phys. Chem. A 103 (1999) 2655.
[179] R.S. MacTaylor, J.J. Gilligan, D.J. Moody, A.W. Castleman, J. Phys. Chem. A 103 (1999) 4196.
[180] E. Herbst, W. Klemperer Phys. Today 29 (1976) 32.
[181] A. Dalgarno, J.H. Black, Rept. Progr. Phys. 39 (1976) 673.
[182] D. Smith, Chem. Rev. 92 (1992) 1473.
[183] See, for example G.B.I. Scott, D.A. Fairley, C.G. Freeman, R.G.A.R. Maclagan, M.J. McEwan, Int. J. Mass Spectrom. Ion Processes 149 (1995) 251.
[184] See, for example G.B.I. Scott, D.A. Fairley, C.G. Freeman, M.J. McEwan, V.G. Anicich, J. Phys. Chem. A 103 (1999) 1073.
[185] D. Smith, P. Spanel, Acc. Chem. Res. 25 (1992) 414.
[186] H.I. Schiff, D.K. Böhme, Astrophys. J. 232 (1979) 740.
[187] D.K. Böhme, in Structure, Reactivity and Thermochemistry of Ions, P. Ausloos, S.G. Lias (Eds.), Reidel, New York, 1987, pp. 219–246.
[188] D.K. Böhme, Nature 319 (1986) 473.
[189] D.K. Böhme, S. Wlodek, H. Wincel, J. Am. Chem. Soc. 113 (1991) 6396.
[190] D.K. Böhme, in Advances in Gas Phase Ion Chemistry, N. Adams, L.M. Babcock (Eds.), JAI Press Inc., Greenwich, Connecticut, 1992, Vol. 1, pp. 225–270.
[191] D.K. Böhme, Chem. Rev. 92 (1992) 1487.
[192] S. Petrie, H. Becker, V. Baranov, D.K. Böhme, Astrophys. J. 476 (1997) 191.
[193] S. Petrie, G. Javahery, D.K. Böhme, Astr. Astrophys. 271 (1993) 662.
[194] S. Petrie, D.K. Böhme, Astr. Astrophys. 540 (2000) 869.
[195] S. Petrie, D.K. Böhme, Mon. Not. R. Astron. Soc. 268 (1994) 103.
[196] J.A. Davidson, C.J. Howard, H.I. Schiff, F.C. Fehsenfeld, J. Chem. Phys. 70 (1979) 1697.
[197] F. Arnold, G. Hauck, Nature 315 (1985) 307.
[198] F. Arnold, G. Knop, Int. J. Mass Spectrom. Ion Processes 81 (1987) 33.
[199] A.A. Viggiano, Mass Spectrom. Rev. 12 (1993) 115.
[200] S.T. Arnold, J. M. Thomas, A.A. Viggiano, Int. J. Mass Spectrom. 179/180 (1998) 243.

[201] A.J. Midey, S.T. Arnold, A.A. Viggiano, J. Phys. Chem. A 104 (2000) 2706.
[202] A. Hansel, A. Jordan, R. Holzinger, P. Prazeller, W. Vogel, W. Lindinger, Int. J. Mass Spectrom. Ion Processes 149/150 (1995) 609.
[203] W. Lindinger, A. Hansel, A. Jordan, Chem. Soc. Rev. 27 (1998) 347.
[204] P. Spanel, D. Smith, Med. Biol. Eng. Comput. 34 (1996) 409.
[205] P. Spanel, D. Smith, Int. Rev. Phys. Chem. 15 (1996) 231.
[206] G.K. Koyanagi, V.I. Baranov, S.D. Tanner, D.K. Böhme, J. Anal. Atom. Spectrom. 15 (2000) 1207.